This is to certify that the
thesis entitled

THE DEPOSITION OF AlN THIN FILMS, THEIR CHARACTERIZATION AND THE FABRICATION OF SURFACE ACOUSTIC WAVE DEVICES

presented by

CHARLEE FANSLER

has been accepted towards fulfillment
of the requirements for the

M.S. degree in Electrical Engineering

Donnie K Reinhard
Major Professor's Signature

5/3/07
Date

THE DEPOSITION OF AlN THIN FILMS, THEIR CHARACTERIZATION AND THE FABRICATION OF SURFACE ACOUSTIC WAVE DEVICES

By

Charlee Fansler

A THESIS

Submitted to
Michigan State University
in partial fulfillment of the requirements
for the degree of

MASTER OF SCIENCE

Department of Electrical and Computer Engineering

2007

ABSTRACT

THE DEPOSITION OF AlN THIN FILMS, THEIR CHARACTERIZATION AND THE FABRICATION OF SURFACE ACOUSTIC WAVE DEVICES

By

Charlee Fansler

This investigation entailed a study of how to fabricate surface acoustic wave (SAW) devices; specifically, the fabrication and design of the electrodes, the thicknesses of the AlN and the UNCD (ultrananocrystalline diamond) layers and the parameters to set for DC pulsed sputter deposition of the AlN layer. The critical layer in the fabrication process is the AlN layer.

The resulting layer of AlN is transparent with an optical gap of approximately 6 eV or 200 nm. Preliminary XRD (x-ray diffraction) results show a small peak signal at 36° for AlN (002) and a significant AlN (004) peak at ~76°. The (002) plane for AlN is the desired plane for its piezoelectric properties. The surface roughness of the AlN layer was low with an Ra of 0.78 nm and an Rz value of 28.77 nm. The deposited layer also had good adhesion to the substrate.

An AlN layer was successfully deposited on UNCD, specifically AlN/UNCD/Si were the order of the layers. Al was also deposited on the AlN layer in order to form the IDTs for the SAW devices. However, it was not possible to etch and pattern the aluminum because the 75 mm diameter wafer was bowed after UNCD deposition. SAW devices were successfully fabricated on a quartz – ST substrate. A signal was obtained for a SAW filter, using an HP 8753D network analyzer, as verification that the SAW devices would work.

For Ashley with lots of love.

ACKNOWLEDGEMENTS

I would like to thank my family for all the support they have given to me over the years; for always expecting more out of me, which motivated me to do more and be better at whatever I was doing. If it weren't for my family I wouldn't be where I am today or be the person that I am now.

I would also like to thank my advisor Dr. Donnie Reinhard for all his help and guidance. I appreciate all that he has done for me and all that he continues to do. I know I could never show the true extent of my gratitude, but I hope this thank you is a good start.

Finally, I would like to thank Dr. Ed Rothwell, Dr. Tim Grotjohn, Dr. Jes Asmussen, and Dr. Thomas Schuelke for their guidance and support along the way. I would like to extend my thanks as well for the support of Michigan State University, the Graduate School and the Fraunhofer Center for Coatings and Laser Applications. I would also like to thank Dr. Percy Pierre and Dr. Barbara O'Kelly, without whom I would not even be in the graduate program.

TABLE OF CONTENTS

LIST OF TABLES

LIST OF FIGURES

Images in this thesis are presented in color.

Chapter 1

Introduction

1.1 Introduction

This chapter gives an overview of this thesis research in general. It will also give a short review of the chapter topics for this thesis. Finally, there will be a summary of this investigation.

1.2 Purpose of Research

A Surface Acoustic Wave (SAW) device is an electronic device which can be used, for example, as a high frequency band-pass filter or an oscillator; for this research filters and oscillators were fabricated and tested. There are many applications for SAW devices. For example, a SAW device may act as a transducer for chemical sensing [1,2,3,4]. SAW devices can also be used in mobile phones, television tuners and optical-communication systems [2,5,6,7,8]. SAW devices are becoming increasingly important in wireless communications. Wireless mobile and fixed transceivers require electronic filters. SAW devices are a great choice for these applications because of their excellent performance and small size. They have high signal selectivity, accurate bandwidths and center frequencies, small transition bandwidths, and low passband ripple [5].

A recent trend in wireless communications is the move toward higher operating frequencies to transmit more information. Current SAW devices not employing diamond as an interlayer are reaching their limitations in operating frequency. The frequency at which a SAW device can operate depends on the material properties of the media being

used to transmit the acoustic wave. For most SAW devices this is the piezoelectric material, which is used to generate the acoustic wave as well. The operating frequency is limited by the phase velocity of the material and the wavelength of the acoustic wave. The wavelength of the acoustic wave is limited by the spacing between the fingers of the IDTs. In order to get higher frequencies the width and spacing of the electrodes must become smaller. In today's fabrication technology the submicron size of the electrodes required to increase the operating frequencies further compromise device reliability and yield [5,9]. Another limitation of SAW devices using conventional materials (i.e. quartz and lithium niobate) is power durability. This becomes more of a problem with the size of the IDTs, the smaller the electrodes the less durable your structure [7,9,10,11].

As technology improves, devices need to operate at higher frequencies and by consequence become smaller in size. As this applies to SAW devices, it has led to research of different materials to avoid reaching the limitations of current lithography techniques to create smaller widths for the IDT electrodes. Diamond, though not piezoelectric, is the material that is the most promising for SAW devices because it has the highest acoustic velocity of any known material. Diamond has a high elastic constant (in this case Young's Modulus) and a high phase velocity as well [5,7]. With an increase in velocity there is an increase in frequency, this will be explained in more detail in Chapter 2. This means that by simply using diamond as an interlayer, between a piezoelectric layer and the substrate, and keeping the same dimensions of the IDTs there is an improvement in performance. Another improvement that could be realized using diamond would be increasing the quality factor (Q) of a resonator. Diamond also has other benefits for use in SAW devices; it has a high thermal conductivity which will

allow for higher power capabilities. SAW devices on diamond have a high electromechanical coupling coefficient, which indicates a high efficiency of energy conversion from the input signal to the SAW [5,7,8,9,10,12,13,14].

For this research we have chosen to use ultrananocrystalline diamond as an interlayer for the SAW devices, between piezoelectric aluminum nitride (AlN) and silicon. Ultrananocrystalline diamond (UNCD) is characterized by a grain size of 2 - 10 nm and is grown by a process developed at Argonne National Laboratories by Gruen and Krauss [15,16]. UNCD has the benefit of a low surface-roughness which will eliminate or greatly minimize the need for polishing the diamond which takes a great deal of time in the fabrication process. This low surface roughness will also minimize propagation loss of the SAW energy which leads to less insertion loss for the device and lower power consumption. Due to the small grain boundaries of the UNCD this lowers the expected acoustic scattering seen at large angle grain boundaries in polycrystalline diamond, especially if grain dimensions are of the same size/length as the acoustic wavelengths, device apertures and transducer separation [17,18]. The thermal conductivity of UNCD however, is low. This could be contributed to the wavelength of the thermal phonons being equivalent to the grain boundaries. However, despite the lower thermal conductivity of UNCD it still offers the potential of diamond-based high frequency performance to SAW devices.

1.3 Chapter Review

Chapter 2 gives an overview of background information needed for understanding this thesis. In this chapter there will be an explanation of piezoelectricity and why it is advantageous in surface acoustic wave (SAW) devices to use diamond as an interlayer.

Next, a description of what a SAW device is, how it works, its applications and some of the performance limitations will be given. Then, a brief description of ultrananocrystalline diamond (UNCD) is given; what are some of its material properties and how it may improve the performance of SAW devices. Next, reasoning is given for the choice of piezoelectric material used for this research. Finally, there is a short review of previous work on diamond based SAW devices.

Chapter 3 explains the procedures used to fabricate the SAW devices. In this chapter, reasoning is given for the choice of film thickness, i.e. what thickness of aluminum nitride to use and what thickness of diamond should be used? Next, there will be an explanation of the design of the electrodes (IDTs) and the process used to fabricate the electrodes (e.g. the deposition of the aluminum, masking and etching). Finally, there will be a discussion on the design of the SAW structures.

Chapter 4 explains the PVD (physical vapor deposition) process of pulse dc sputtering, what is it/how does it work and why is it important, as compared to other sputtering methods. There will be a description of the sputtering system used, that was developed by Kurt J. Lesker, and of the operating procedures. Finally, there will be a discussion of the results of sputtering an aluminum nitride (AlN) layer on a Si substrate; there will be a comparison of the properties of the sputtered layer vs. the sputtering parameters.

Chapter 5 will discuss the observations made after the AlN deposition. First, a discussion of general observations made, such as measurements concerning surface roughness, substrates used and deposition parameters. Next, characteristics of the film that will be discussed are growth rate, uniformity and adhesion. Optical data,

transmission and reflection, was also collected. Then, x-ray diffraction (XRD) was used to determine the chemical composition and lattice structure of the deposited layer. Finally, scanning electron microscopy (SEM) was used to determine grain growth.

Chapter 6 will summarize the results for this investigation. In this chapter conclusions from these results will be made. Finally, suggestions for the possibility of future work will be made as well.

1.4 Summary

This thesis investigates the fabrication of SAW devices and the deposition of a piezoelectric thin film layer of AlN for the proper function of the SAW device. There is also a discussion of the benefits of using diamond, specifically UNCD, as an interlayer for the SAW device to improve the function of the device. Simply by having the diamond interlayer in place without making any other changes to the device improves its functional capabilities due the material properties of diamond.

The background material, such as piezoelectricty, coupling factors, and previous works with diamond and SAW devices is discussed. Then the design process is discussed in detail, the thickness of specific layers that must be used in order to optimize the function of the SAW device using the diamond interlayer, the design of the electrodes and their fabrication and the design of the SAW devices themselves. The operation of the Kurt J. Lesker PVD75 system will be discussed, how it works and procedures for deposition. Finally, there will be a discussion of deposition observations and characterization of the AlN thin film layer.

Chapter 2

Background

2.1 Introduction

This chapter gives an overview of background information needed for understanding this thesis. In this chapter there will be an explanation of piezoelectricity and key related material parameters. Next, a description of what a SAW device is, how it works, its applications and some of the performance limitations will be given. Then, a brief description of ultrananocrystalline diamond (UNCD) is given; what are some of its material properties and how it may improve the performance of SAW devices. Next, reasoning is given for the choice of piezoelectric material used for this research. Finally, there is a short review of previous work on diamond based SAW devices.

2.2 Piezoelectricity

Piezoelectric material has the property that when a mechanical stress is put on the material it creates an electric field. Conversely, if an electric field is applied to the material it produces a change in dimensions. In other words, the piezoelectric material transforms mechanical energy into electrical energy in a reversible process. The molecules in the crystal are polarized but are symmetrically distributed so that the charge of the crystal is neutral. When an electric field is applied to the material the molecules align themselves with the field causing a change in dimensions. If a mechanical stress (a change in dimensions) is applied to the material the charges of the molecules are no longer symmetrically distributed and charges of opposite polarity build up on either side

of the material creating an electric field across the material. For example, if electrodes are placed on a piezoelectric material and a time varying voltage is applied to them (as shown below in Figures 1 and 2) this creates a time varying electric field and this in turn induces a time varying stress in the piezoelectric material. There is also a time-varying strain associated with the stress due to the opposite polarity of the electrodes. This time-varying stress and strain is the excitation of a surface acoustic wave; which means that when applying electrical energy to a piezoelectric material it is converted to mechanical energy, as mentioned previously.

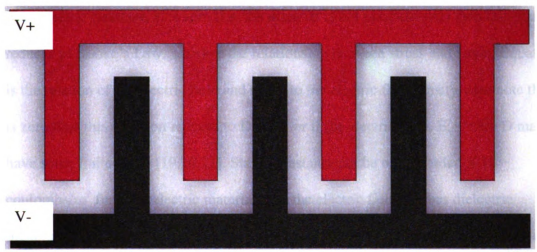

Figure 1 Time varying voltage applied to electrodes on a piezoelectric substrate (top view)

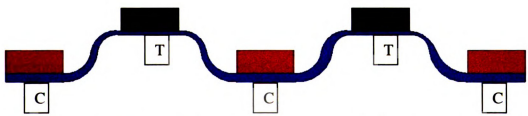

Figure 2 Tension and compression due to time varying voltage (side view)

Piezoelectricity can be described mathematically using the following piezoelectric stress equations:

$$T = cS - e\mathrm{E} \tag{1}$$

$$D = \varepsilon\mathrm{E} + eS \tag{2}$$

where T is stress, S is strain, c is the elastic stiffness constant, e is the piezoelectric stress constant, E is the electric field, ε is permittivity and D is the electric flux density. These equations are simplified versions of the true representations (for ease of understanding); the elastic, piezoelectric and permittivity constants are tensors. Using crystal symmetry these independent elements are limited in number in specific cases [19]. Equation 1 is the relation of the strain and the electric field to the mechanical stress. Notice that if the piezoelectric constant, e, is zero (i.e. the material is not piezoelectric) then this equation reduces to Hooke's Law, which is the relationship between stress and strain. Equation 2 is the relation of the electric field and strain to the electric flux density; also note that if e is zero then this equation reduces to D = εE, or if the electric field, E, is zero D may still have some finite value [19,20,21]. Stress constants can be on the order of 10 coulombs/m^2 for piezoelectric materials. As the electric field reaches dielectric breakdown voltages on the order of 10^7 volts/m the induced stress can be as large as 10^8 Pa [20].

How efficiently the piezoelectric material converts mechanical energy to electrical energy, and vice-versa, is measured by the coupling constant. The electromechanical coupling coefficient, K, is defined as follows:

$$K^2 = \frac{MechanicalEnergy}{ElectricalEnergy} \tag{3}$$

For bulk materials and bulk acoustic waves, K can be calculated in closed form using material properties. Due to the surface acoustic waves' inhomogeneity in the z-direction (perpendicular to the surface), there is no corresponding explicit electromechanical

coupling factor [19]. The electromechanical coupling efficiency, for even the strongest piezoelectric material, is only about 5%, but this is high enough to be practical and is the basis for surface acoustic wave devices.

2.3 Surface Acoustic Wave Device

A Surface Acoustic Wave (SAW) device is an electronic device which can be used, for example, as a high frequency band-pass filter or an oscillator; for this research filters and oscillators were fabricated and tested. A simple SAW device consists of interdigital transducers (IDT) and a piezoelectric material (i.e. quartz, zinc oxide or aluminum nitride). An example of a simple SAW filter is shown below in Figure 3.

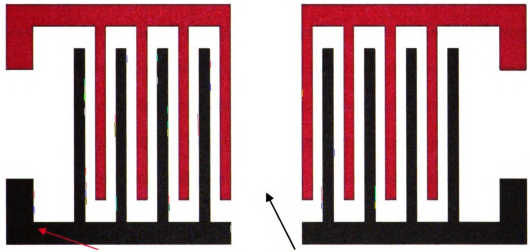

Figure 3 Simple SAW device (filter)

The piezoelectric material used for the SAW devices in this thesis is aluminum nitride (AlN).

An interdigital transducer (IDT) is a metal structure of interleaved electrodes (also referred to as fingers) with each set connected to a common contact pad, as shown in Figure 3. The input IDT is used to initiate surface acoustic wave in a material and the

output IDT is used to detect a voltage. A time varying voltage is applied to the input IDT; this creates a periodic distribution of an electric field. Using the appropriate frequency of applied voltage, the period is correlated to the spacing between the fingers of the IDT. This field then causes a mechanical stress on the piezoelectric material which creates a surface acoustic wave. This wave travels through the material to another IDT which detects a voltage induced from the mechanical stress of the surface wave.

There are many applications for SAW devices. For example, a SAW device may be coated with organic or inorganic material which allows analytes to be sorbed to the device surface and the SAW device to act as a transducer for chemical sensing [1,2,3,4]. SAW devices can also be used in mobile phones, television tuners and optical-communication systems [2,5,6,7,8]. SAW devices are becoming increasingly important in wireless communications. Wireless mobile and fixed transceivers require electronic filters. SAW devices are a great choice for these applications because of their excellent performance and small size. They have high signal selectivity, accurate bandwidths and center frequencies, small transition bandwidths, and low passband ripple [5].

A recent trend in wireless communications is the move toward higher operating frequencies to transmit more information. Current SAW devices not employing diamond as an interlayer are reaching their limitations in operating frequency. The frequency at which a SAW device can operate depends on the material properties of the media being used to transmit the acoustic wave. For most SAW devices this is the piezoelectric material, which is used to generate the acoustic wave as well. The operating frequency is limited by the phase velocity of the material and the wavelength of the acoustic wave. The wavelength of the acoustic wave is limited by the spacing between the fingers of the

IDTs. The relationship between finger width/spacing and wavelength is shown in Equation 5 on the following page. In order to get higher frequencies the width and spacing of the electrodes must become smaller. In today's fabrication technology the submicron size of the electrodes required to increase the operating frequencies further compromise device reliability and yield [5,9]. Another limitation of SAW devices using conventional materials (i.e. quartz and lithium niobate) is power durability. This becomes more of a problem with the size of the IDTs, the smaller the electrodes the less durable the structure [7,9,10,11].

2.4 Diamond Interlayer for SAW Device

As technology improves, devices need to operate at higher frequencies and by consequence become smaller in size. As this applies to SAW devices, it has led to research of different materials to avoid reaching the limitations of current lithography techniques to create smaller widths for the IDT electrodes. Diamond, specifically, is the material that is the most promising for SAW devices because it has the highest acoustic velocity of any known material. The acoustic velocity of a bulk material is related to the elastic constant in the following equation,

$$v = \sqrt{\frac{c}{\rho}} \tag{4}$$

where v is the phase velocity, c is the elastic constant of the material and ρ is the density of the material . It can be seen that as c increases v increases as well. Diamond has a high elastic stiffness constant (also called Young's Modulus) and, based on the relation of c and v in Equation 4, a high phase velocity as well [5,7]. The phase velocity for diamond has been calculated to be approximately 18,000 m/s, for the longitudinal velocity, and

between 10,500 – 13,000 m/s for the two shear velocities [22]. This is important because the frequency of the device is related to velocity by the equation,

$$f = \frac{v}{\lambda} \tag{5}$$

where f is the frequency, v is the phase velocity and λ is the wavelength [1,5,7,9,11,17,18,23,24,25,26]. As can be seen from this equation, with an increase in velocity there is an increase in frequency. This means that by simply using diamond as an interlayer, in a SAW device, and keeping the same dimensions of the IDTs there is an improvement in performance. The width and spacing of the IDTs is related to the wavelength of the acoustic wave by the equation:

$$IDT_{width} = \frac{\lambda}{4} \tag{6}$$

[5,7,18]. This means by using a larger width for the fingers on a SAW device with diamond as an interlayer the same frequency can be achieved as with fingers of a smaller width on SAW devices without diamond as an interlayer. Another improvement that could be realized using diamond would be increasing the quality factor (Q) of a resonator which can be approximated by the equation:

$$Q = \frac{f_o}{\Delta f} \tag{7}$$

where f_0 is the operating (center) frequency and Δf is the full width at half maximum value of the peak [27]. Diamond also has other benefits for use in SAW devices; it has a high thermal conductivity which will allow for higher power capabilities. SAW devices on diamond have a high electromechanical coupling coefficient, which indicates a high efficiency of energy conversion from the input signal to the SAW [5,7,8,9,10,12,13,14].

For this research we have chosen to use ultrananocrystalline diamond as an interlayer for the SAW devices. Ultrananocrystalline diamond (UNCD) is characterized

by a grain size of 2 - 10 nm and is grown by a process developed at Argonne National Laboratories by Gruen and Krauss [15,16]. UNCD has the benefit of a low surface-roughness which will eliminate or greatly minimize the need for polishing the diamond which takes a great deal of time in the fabrication process. This low surface roughness will also minimize propagation loss of the SAW energy which leads to less insertion loss for the device and lower power consumption. Due to the small grain boundaries of the UNCD this lowers the expected acoustic scattering seen at large angle grain boundaries in polycrystalline diamond, especially if grain dimensions are of the same size/length as the acoustic wavelengths, device apertures and transducer separation [17,18]. The thermal conductivity of UNCD however, is low. This could be contributed to the wavelength of the thermal phonons being equivalent to the grain boundaries. However, despite the lower thermal conductivity of UNCD it still offers the potential of diamond-based high frequency performance to SAW devices.

2.5 Piezoelectric Material for SAW Device

Due to the fact that diamond is not piezoelectric, a piezoelectric material must be used to excite a SAW which may then propagate along and near the surface of the diamond interlayer. Surface acoustic waves, as the name suggests, travel on or near the surface of the medium. The atoms in the medium have an elliptical shaped displacement and this displacement drops to zero within a few wavelenths [5]. Using a thin-film overlayer can cause high dispersion for sound propagation and admits a multiplicity of allowed modes. However, successful devices using layered structures with diamond as an interlayer have been reported [18]. AlN is the piezoelectric material used for this research. It has the ability to be sputtered on a substrate in a reactive environment and no

special equipment is required to accomplish this; unlike the case for zinc oxide (ZnO) which needs a special vacuum pump in order to sputter in the reactive environment with oxygen. Sputtering aluminum nitride also does not require the removal of hazardous waste gases. Aluminum nitride with a diamond interlayer when compared with zinc oxide with a diamond interlayer has a higher acoustic velocity and a higher electrical resistivity [17].

2.6 Previous Work on Diamond Based SAW Devices

Currently there are two groups who have studied SAW structures using UNCD as an interlayer to take advantage of its high acoustic velocity [17,18]. Bi, Huang, Asmussen and Golding [18] studied a layered system of ZnO/UNCD/Si to determine the use of UNCD as a possible substrate for SAW devices. It was found that several modes exist for a given value of kh_{ZnO} and that they are highly dispersive at small values of kh_{ZnO}. For large normalized thickness (kh, where k is $2\pi/\lambda$ and h is the thickness of the ZnO) of the ZnO layer the phase velocity of the Rayleigh wave approached that of ZnO and as kh_{ZnO} approached zero the velocity of the Rayleigh wave approached that of diamond. It was also shown that the SAW devices on UNCD and on polycrystalline diamond substrates are indistinguishable, within combined uncertainties [18]. Bénédic, et al [17], reported for the first time the successful fabrication of AlN/UNCD/Si layered structure based SAW devices. It was shown that, related to the wave penetration depth, the acoustic velocity depends on the IDTs periodicity and on UNCD film thickness; this means that by reducing the IDT finger size, there is no need for a thick layer of UNCD films to eliminate the silicon substrate influence. A SAW velocity of 9,500 m/s was realized for

an UNCD layer of 19 μm thick and a wavelength of 32 μm. This velocity is higher than the velocity obtained for the 0^{th} Rayleigh mode ZnO/UNCD/Si structure [17].

Several investigations have studied SAW structures with non-UNCD diamond. Elmazria, et al [23], investigated fabricating high velocity SAW devices using AlN on CVD diamond. They found that using their technique there was a good combination of high electromechanical coupling coefficient and temperature coefficient of frequency (TCF). TCF is the measure of the stability of the frequency with a change in temperature and it was noted that as kh_{AlN} (which is the wave number times the thickness of the AlN layer) increases the TCF decreases, which means greater operating frequency stability as temperature changes [23].

Iriarte, et al [28], using parameter extraction, found that for a 4.3 μm thick layer of AlN film deposited on polycrystalline diamond the SAW velocity was about 10,000 m/s and for thinner films of about 2 μm thick the velocity increased to about 11,800 m/s. This means that SAW devices operating in the microwave region are feasible using standard fabrication techniques. It was also shown that there is a relatively high effective coupling coefficient of about 1% [28].

Higaki, et al [10], investigated the high power durability of a ZnO/diamond/Si based SAW filter as compared to a $LiTaO_3$ (lithium tantalate). It was shown that the ZnO/diamond filter operating at 2.9 GHz, maintained linearity up to the input power of 36 dBm. The $LiTaO_3$ filter operating at 822 MHz was nonlinear above 23 dBm and incurred severe damage at input power of 27.7 dBm. The ZnO/diamond filter operating at a frequency 3.5 times higher than the $LiTaO_3$ filter was able to withstand 8 dBm higher

input power than that of the $LiTaO_3$ filter as well. These results are assumed to be due to the high thermal conductivity and structural integrity of diamond [10].

Although this is not an exhaustive review of previous diamond based SAW device work, it does provide a sampling of background work pertinent to this thesis. This thesis further explores materials and device fabrication issues relative to AlN/UNCD SAW structures.

Chapter 3

SAW Fabrication Considerations and Procedure

3.1 Introduction

This chapter will explain the procedures used to fabricate the SAW devices. In this chapter, reasoning is given for the choice of film thickness, i.e. what thickness of aluminum nitride to use and what thickness of diamond should be used? Next, there will be an explanation of the design of the electrodes (IDTs) and the process used to fabricate the electrodes (e.g. the deposition of the aluminum, masking and etching). There will be a discussion on the design of the SAW structures. This chapter will also give a physical description of the network analyzer used to characterize the SAW devices. An explanation will be given of the operating and calibration procedures and a description of the probe station and probes, which are part of the characterization setup. Finally a discussion of the results obtained from aluminum electrodes fabricated on quartz.

3.2 Film Thickness Considerations

The film thickness of the multiple layers of the SAW device is a critical factor when designing the device. It is important because, as the name suggests, surface acoustic waves travel along and near the surface of the material but disperse rapidly to zero within a few wavelengths from the surface [1,5,19,29,30]. The thickness of the diamond is important because it needs to be thick enough so that the silicon substrate beneath it does not affect the velocity of the acoustic wave and so that negligible acoustic energy is lost to the silicon substrate. The thickness of the aluminum nitride is important because it is

related to the electromechanical coupling coefficient and the overall SAW velocity. The desired thickness of the diamond and the aluminum nitride layers were found based on theoretical calculations by Benetti, et al [30] and Nakahata, et al [14]. The layers for the SAW device are as shown in Figure 4.

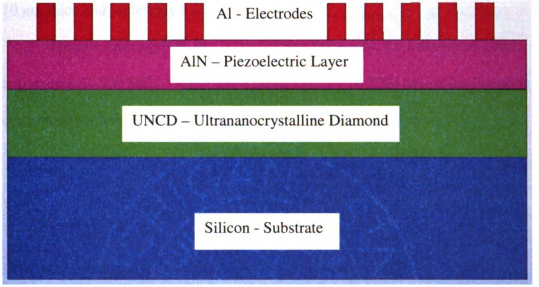

Figure 4 SAW device layers

The layer of diamond needs to be thick enough so that the silicon layer has no effect on the performance of the SAW device; specifically on the dispersion of the SAW and the velocity of the SAW. From previous work [14], a minimum normalized diamond thickness of 4 is appropriate for phase velocity considerations,

$$kh_{dia} \geq 4 \tag{8}$$

where $k = 2\pi/\lambda$ and h is the thickness of the diamond. From Nakahata, et al [14], the velocity of the surface wave does not appreciably increase for thicker diamond layers. Utilizing a normalized thickness of ≥4, in a layered system, yields a near maximum phase velocity. For this research we chose a wavelength of 16 μm; inserting this into the equation 8 gives a minimum thickness of approximately 10 μm for the diamond layer.

Additionally, as mentioned previously, energy can be lost to the silicon if the diamond is too thin. Benetti, et al [30], recommend that the diamond be "at least a few acoustic wavelengths," thick to avoid energy loss to the silicon, which would correspond, in our case, to 48 μm using a thickness of 3λ. In summary, the diamond film should be at least 10 μm thick and preferably thicker.

For this investigation, the desired center frequency, for a device on quartz, is approximately 500 MHz. Quartz has a phase velocity of 3200 m/s; using Equation 5, the corresponding wavelength is found (as shown below) to be 16 μm.

$$\lambda = \frac{3.2x10^3 m/s}{5.0x10^8 /s}$$

$$\lambda = 16\mu m$$

Now, using Equation 6 the width of the IDT's was found, as shown below.

$$IDT_{width} = \frac{16\mu m}{4}$$

$$IDT_{width} = 4\mu m$$

These parameters, wavelength and IDT width, were then used to find the necessary thickness for the diamond layer. Using Equation 8 and the relation $k = 2\pi/\lambda$, the minimum thickness for the diamond was found, the calculations for this are shown below.

$$k = \frac{2\pi}{16}$$

$$k \approx 0.4$$

$$h_{dia} \geq \frac{4}{0.4}$$

$$h_{dia} \geq 10\mu m$$

The thickness of the AlN is important as well, because if the AlN is too thick the SAW will not reach the diamond and the full benefits of having the diamond layer will not be realized. The electromechanical coupling coefficient also depends on the AlN thickness. For analyzing, the thickness of the AlN (aluminum nitride) the same normalization (kh) is used. Benetti [30] has calculated K^2 values versus AlN thickness for semi-infinite diamond and Nakahata has calculated K^2 values versus ZnO (zinc oxide) thickness for thinner diamond layers. Based on the former, a normalized thickness of 0.2, for AlN is used; this is where the maximum coupling coefficient is realized (for the layered structure used in this research)

For a semi-infinite diamond layer and a normalized AlN thickness of 0.2, the theoretical velocity of approximately 8500 m/s for the Rayleigh mode; higher velocities and coupling coefficients can be obtained for the Sezawa modes [30]. Using equation 5 (in Chapter 2) and substituting in the above mentioned phase velocity and a wavelength of 16 μm, the operating frequency of the SAW device should be about 531 MHz. The maximum coupling coefficient calculated for this layered structure is $K^2 = 0.0015$ or 0.15%.

3.3 Electrode (IDT) Formation

The fabrication of the electrodes is a multi-step process. Figure 5, shown on the following page, illustrates the step-by-step process of fabricating the electrodes.

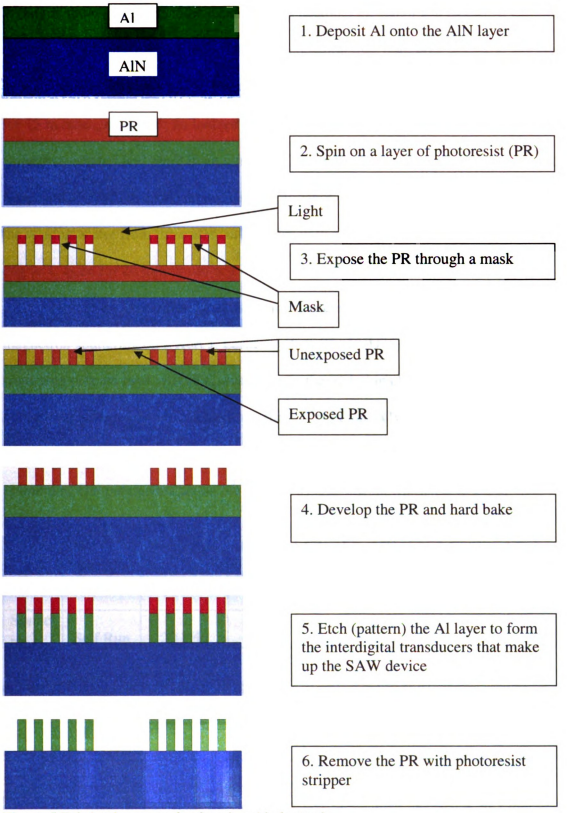

Figure 5 Fabrication steps for forming Al electrodes

To begin, the wafer needs to be cleaned using acetone, methanol and isopropyl alcohol. If the wafer is not clean before the aluminum deposition then both poor adhesion and breaks in electrode patterns may result. Place the wafer in acetone and put it in an ultrasonic bath for 15 minutes, rinse with de-ionized water and dry with a nitrogen gun. Then place the wafer in methanol and put it in an ultrasonic bath for 15 minutes, rinse with de-ionized water and dry with a nitrogen gun. Use isopropanol (isopropyl alcohol, IPA) to evaporate the residual water from the wafer surface, dry with a nitrogen gun and put into a 120 degree C oven for 20 minutes to dry.

Next is the deposition process, which is accomplished using DC pulsed magnetron sputtering on a Kurt J. Lesker system (the PVD75). This system and the sputtering process used will be discussed in further detail in chapter 4. The PVD75 system was pumped down to a base pressure of less than $4x10^{-6}$ Torr, the chamber pressure during sputtering was set to 3 mTorr and argon was used to sputter the aluminum. The parameters set on the PVD75 system are shown in Table 1 – 3.

Table 1 Parameters for the Sparc-le V unit in the PVD75

	Arc Handling	**Frequency**	**Reverse Time**	**Crowbar Delay**	**Reverse Voltage**	**Control Mode**	**Substrate Rotation**
Sparc-le V	Self Run	20 kHz	3 μs	10 μs	10 %	Local	5

Table 2 Parameters for the MDX 1.5 kW power supply to the cathode of the PVD75

	Power (Constant Power Mode)	**Ramp Time**
MDX 1.5 kW (Power Source)	800 W	5 s

Table 3 Parameters for inside the chamber of the PVD75

	Base Pressure	**Operating Pressure**	**Gas Flow** (Argon)
Chamber	$< 4*10^{-6}$ Torr	3 mTorr	Mode 2

An explanation of parameter settings will be given in more detail in Chapter 4 when the operation of the PVD75 will be explained in detail. Only a thin layer, approximately 200 nm, of aluminum is needed to fabricate the electrodes. Using the above parameters, the deposition rate for aluminum is about 55 nm/min; in order to deposit 200 nm of aluminum then the power supplied to the target needs to run at 800 W for about 4 minutes.

Next, to form the IDTs and hence the SAW device, the aluminum needs to be patterned. To pattern the aluminum the substrate needs to be coated with photoresist (a light sensitive material), which once exposed to light through a mask (blocks the light in a specified pattern) will create the desired pattern when it is developed. Before coating the wafer it must be cleaned to ensure that the electrodes form properly and don't end up with defects such as breaks in the electrodes. The wafer is cleaned using the acetone, methanol and IPA procedure mentioned previously. The substrate is then coated with a thin layer of AZ ADH Promoter, for better adhesion of the photoresist to the surface, using a 5 mL pipette. A programmable spinner is used to spin off the excess promoter and creates a thin and uniform layer of promoter across the wafer. Using the spinner ensures that the layer spun on is the desired thickness, determined by the time and rate of rotation, and ensures that the layer is uniform. The promoter is spun on at 3000 rpm for 30 seconds. Next, the substrate is then coated with S1813 positive photoresist. Positive photoresist means that when it is exposed to light the photoresist rinses away when it is developed. The wafer is covered with a thin layer of photoresist using a 5 mL pipette, spun for 30 seconds at 3000 rpm and the resulting layer of photoresist is approximately 1.23 μm thick. The thickness of this layer is important because the thicker the photoresist

is the longer it needs to be exposed, or a higher power of exposure is required to ensure that the light penetrates the entire layer of photoresist. However, if the layer of photoresist is too thin it will not resist the acid etch used to pattern the Al. The substrate is then soft baked in a 70 degree C oven for 20 minutes.

Next, the photoresist is masked, exposed and developed in order to pattern the photoresist which will eventually pattern the aluminum and form the SAW devices. Two masks were designed. A SAW Mask was designed with 4 and 6 μm width electrodes and a Backup SAW Mask was designed with 8 μm width electrodes in the event that the dimensions on the SAW Mask could not be attained. Each mask has 24 die on it and each die has 5 different devices. The die is copied 23 times to make up the rest of the 24 die. The devices and their designs will be explained in the next section. The SAW Mask is shown on the next page in Figure 6. The Backup SAW Mask has the same general form, 7 rows of die with a total of 24 die.

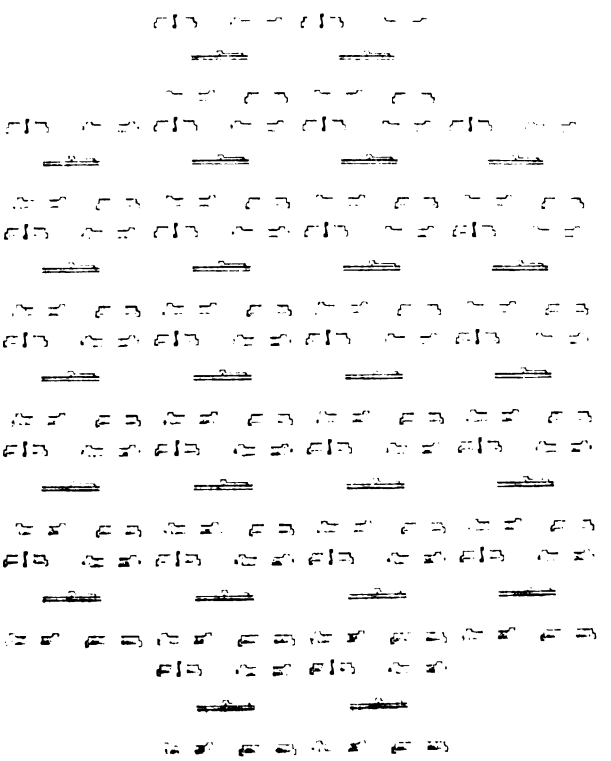

Figure 6 SAW Mask with 24 die, each with 5 devices

The wafer is exposed to UV light for 1.3 minutes using a Karl Suss MJB3 mask aligner. The wafer is then placed in 50 mL of MF-319 developer for approximately 60 seconds. The developer removes the photoresist which has been exposed to light and has no effect on the photoresist which was not exposed. The substrate is rinsed with DI water, a nitrogen gun is used to remove the excess water and then it is hard baked in a 110 degree C oven. The hard baking process hardens the photoresist so that it can withstand the acid etch.

Now the aluminum can be etched in the pattern of the photoresist. An aluminum etchant (consisting of 80 mL of phosphoric acid, 10mL of water, 5 mL of nitric acid and 5 mL of acetic acid) is heated and the wafer is left in the etchant for 2 minutes or until all of the exposed (not covered by photoresist) aluminum has been etched away. Extreme

care must be taken during this step, so that the aluminum is not over etched. If the aluminum is over etched then undercutting can cause the finger width to decrease or may cause the fingers to be etched away completely. If this happens the SAW device will not work as expected or may not work at all. Now that the aluminum has been etched, not only are the IDTs formed but now the SAW devices have been created as well.

3.4 Electrode (IDT) Design

In order to fabricate a working SAW device, there must be a way to excite a surface acoustic wave in the piezoelectric material. Exciting a surface acoustic wave is achieved using IDTs which are formed with contact pads, a bus bar and electrodes (also referred to as fingers). The distance between the IDTs, the number of electrodes, length, overlap and width are designed to obtain the desired performance of the SAW device.

For this investigation, the parameters listed above are based on previous works [16,17,28]. Fifty pairs of electrodes were used for each IDT (input and output) for the filters and a total of 200 pairs of electrodes were used for the oscillators. The distance between input and output IDTs is 1 mm. The length of the electrodes is approximately 500 μm and the overlap distance of the electrodes is 492 μm. The width (and spacing) of the electrodes has an effect on the wavelength of the SAW. The width of the IDT is related to the wavelength by equation 6, as noted in Chapter 2. This means the IDT width can be calculated for a given wavelength [5,7,18,25]. In this research, an IDT width and spacing of approximately 4 μm was used, based on a desired wavelength of 16 μm. There are also other parameters pertaining to the electrodes and IDTs which can be optimized for performance of the SAW which are beyond the scope of this research. The designs

used for the filters and oscillators were taken from a commercially produced SAW device.

Five different structures were made altogether; close up views of the devices are shown below in Figure 7 and Figure 8. Both the SAW Mask and the Backup SAW Mask are shown; Figure 7 is the SAW Mask and Figure 8 is the Backup SAW Mask.

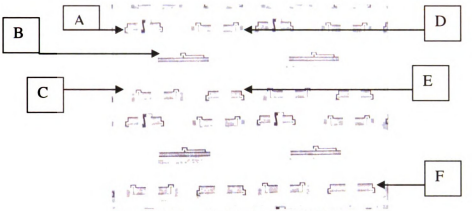

Figure 7 Four die on the SAW Mask

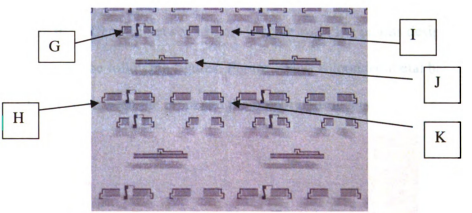

Figure 8 Four die on the Backup SAW Mask

The significant difference between the SAW Mask and the Backup SAW Mask are the widths of the fingers and the number of fingers on the IDTs. In Figure 7, A, C, D and E are filters that have electrodes 4 μm wide and have 50 pairs of electrodes per IDT; the filter labeled F has electrodes 6 μm wide and has 50 pairs of electrodes per IDT; the oscillator labeled B has 200 pairs of finger and has 73 reflectors (gratings) that are 4 μm

wide on each end. In Figure 8, G and I are filters that have electrodes 8 μm wide and have 20 pairs of electrodes per IDT; the filters labeled H and J have electrodes 8 μm wide and have 40 pairs of electrodes per IDT; the oscillator labeled J has 100 pairs of electrodes.

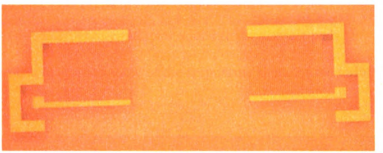

Figure 9 Filter with 20 electrode pairs per IDT at 8 μm wide

In Figure 9, above, is a filter from the Backup SAW Mask. The contact pads for the devices are designed with dimensions compatible with the high frequency probes used to probe the devices for characterization. From the top arrow to the bottom arrow the contact pads are ground, signal, ground. Figure 9 shows the basic design for the filters on both masks and the difference between filters is some variation on this design. These variations are shown in the following figures. Figure 10 has a gounded metal bar placed approximately halfway between the input and the output transducers.

Figure 10 Filter with 50 electrode pairs per IDT at 4 μm wide

Figure 11, shown on the following page, the filter has a serpentine inductor attached to the signal and ground contact pad of the IDT. There is an inductor attached to each of the IDTs.

Figure 11 Filter with a serpentine inductor added to the contact pads

Figure12, below, is a magnified view of the serpentine shape of the inductors attached to either IDT.

Figure 12 View (50x) of serpentine inductor attached to contact pads of filter

Figure 13 shows a filter with another serpentine type inductor attached to either IDT. This inductor design was copied from a commercial SAW device.

Figure 13 Filter with grated, serpentine inductor attached to contact pads of filter

Figure 14 is a magnified view of what the inductor looks like and shows how it differs from the simple design of the inductor shown in Figure 12. The inductor shown in Figure 14, on the following page, has gratings in the length of the inductor; the inductor in Figure 12, above, is simply a length of solid metal.

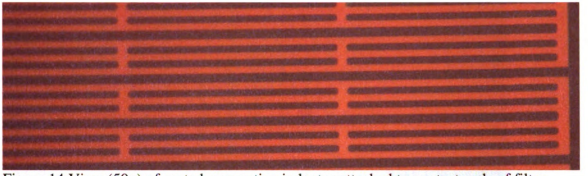

Figure 14 View (50x) of grated, serpentine inductor attached to contact pads of filter

Figure 15, shown below, is the general design for the oscillators and the difference between the oscillators on the two different masks is the width and number of electrodes and the width and number of reflectors at each end.

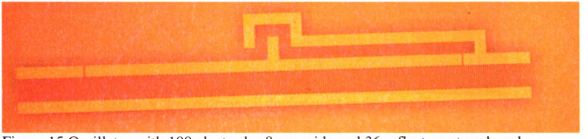

Figure 15 Oscillator with 100 electrodes 8 μm wide and 36 reflectors at each end

The design of the IDTs for this research has been simplified, in one important regard, from the design used in the commercial device. The electrodes used in this research are uniform, meaning they are all the same size, shape, length and width. A simplified view of the IDT design for this research is shown in Figure 3. The electrodes for the commercial device are of different lengths forming the shape of a sinc function. A drawing of the IDT design for the commercial device is shown on the following page in Figure 16.

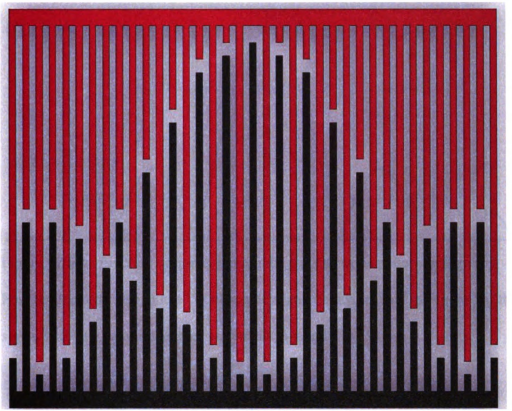

Figure 16 IDT design of the commercial device used in this investigation

The simplified design of the IDT was used instead of the commercial design, in order to simplify the process of designing the mask. The difference in the designs of the electrodes affects the impulse response (transfer function) of the filter. The output signal of the filter is related to the Fourier transform of the overlap of the electrodes that make up the IDTs. This means that for the design of electrodes shown in Figure 1 the output signal will be a sinc function as shown in Figure 17.

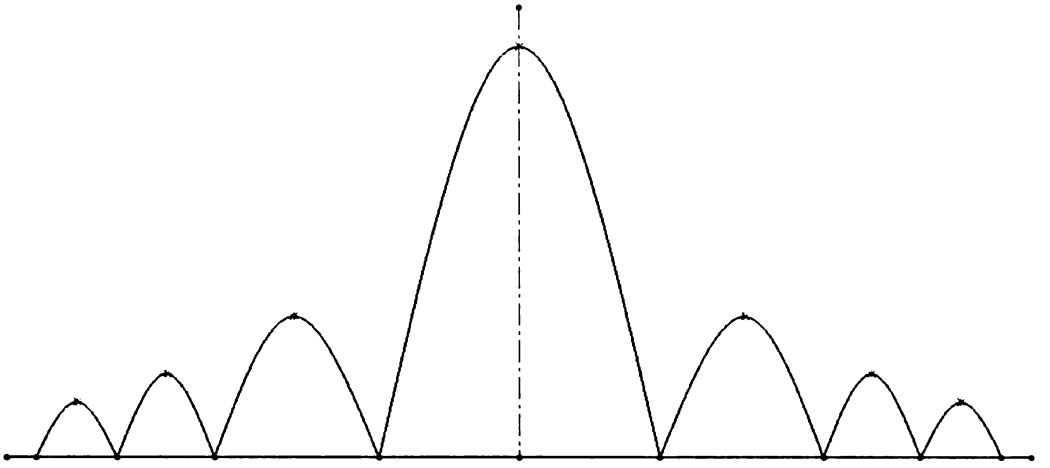

Figure 17 Sinc function output corresponding to electrode pattern in Figure 1

For the electrode design used in the commercial device (shown in Figure 16) the output signal will be a bandpass signal as seen in Figure 18 [5,19].

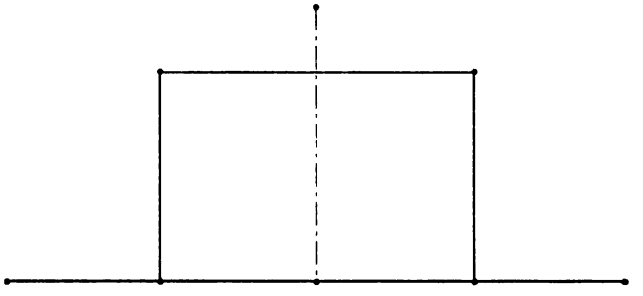

Figure 18 Band pass output corresponding to electrode design in Figure 16

Chapter 4

Aluminum Nitride Deposition and Characterization

4.1 Introduction

This chapter will explain the PVD (physical vapor deposition) process of pulse dc sputtering, what is it/how does it work and why is it important, as compared to other sputtering methods. There will be a description of the sputtering system used, that was developed by Kurt J. Lesker, and of the operating procedures. Finally, there will be a discussion of the results of sputtering an aluminum nitride (AlN) layer on a Si substrate; there will be a comparison of the properties of the sputtered layer vs. the sputtering parameters.

4.2 Pulse DC Sputtering

There are different types of sputtering methods; for example, dc, rf (or ac), reactive, magnetron and other variations and combinations of these methods. In this investigation we used pulsed dc magnetron sputtering in a reactive process in order to produce a thin film of AlN on our substrate. For pulse dc magnetron sputtering, there is a negative dc voltage applied to the planar circular cathode, which is where the target sits. A cross-section of the chamber setup is shown on the following page in Figure 19.

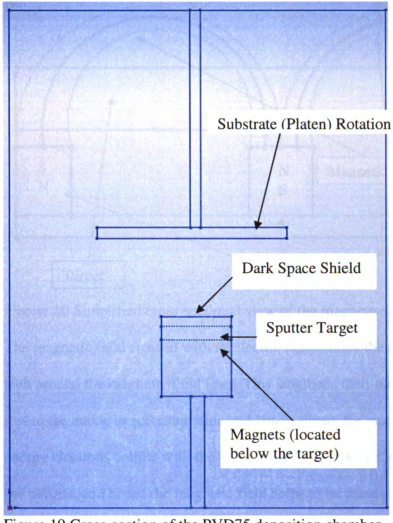

Figure 19 Cross-section of the PVD75 deposition chamber

Under the target and cathode there are also magnets. One magnet is centered under the target and a magnet of opposite polarity encircles the perimeter of the target. This set up creates magnetic field lines from the center of the target to the perimeter of the target. Figure 20, below, shows a simplified cross-section of the magnetic field lines.

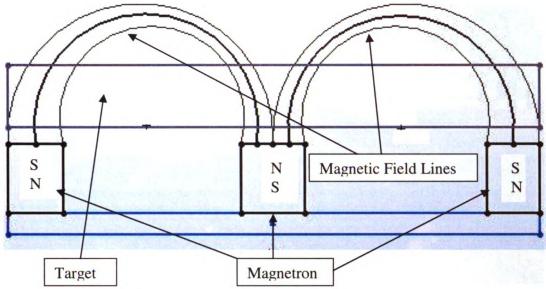

Figure 20 Simplified cross-sectional view of the magnetron's magnetic field lines

The magnetic field crossed with an electric field causes the electrons to travel in a helical path around the magnetic field lines. This lengthens their mean free path before they are lost to the anode or recombination and hence allows for more collisions [31]. The high energy electrons collide with the argon atoms and produce ions, and other species within the plasma, and hence the magnetic field helps to increase ionization in the area where the field exists. These ions are then accelerated towards the target and eject atoms from the target when striking it. The atoms are adsorbed to the surface of the substrate but the atoms travel in all directions and coat other surfaces of the chamber as well. The localized ionization in the region of the magnetic field lines causes the plasma to form in a ring shape (also called a race track) on the target as shown below in Figure 21.

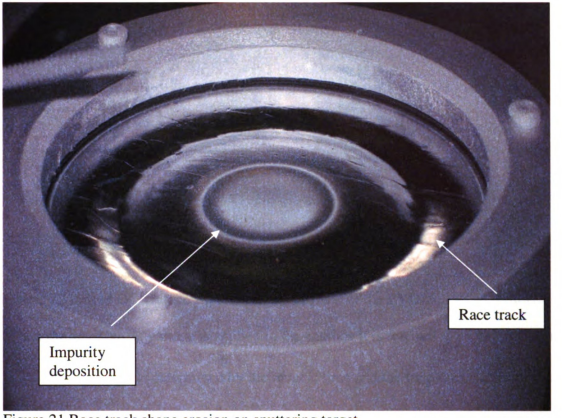

Figure 21 Race track shape erosion on sputtering target

As sputtering occurs some particulates, insulating layers and impurities get deposited onto the target as well as other surfaces in the chamber, which can be seen in Figure 21. These impurities cause a charge to build up on the target (and other surfaces). In order for the charge build-up to be discharged an arc occurs. These arcs can either be hard arcs or micro-arcs. A micro-arc is an arc that is eliminated with one reverse pulse and a hard arc is one that is eliminated with multiple reverse pulses [32]. The pulsing frequencies are usually between 10 and 350 kHz and the duty cycles are commonly between 50-90% [33]. A diagram of the pulsing voltage is shown below in Figure 22.

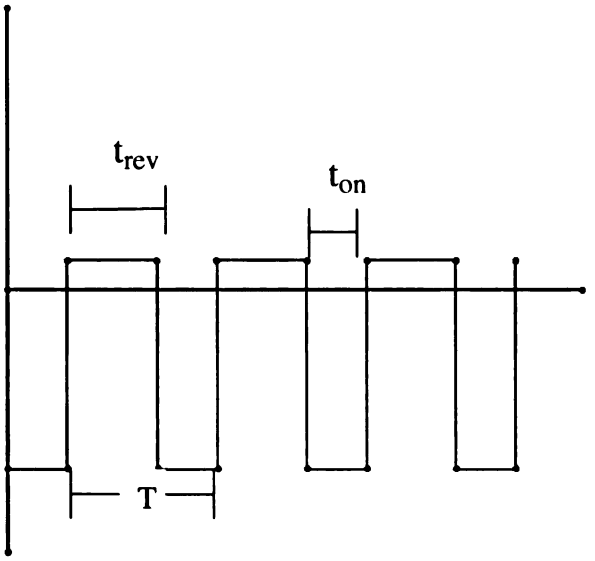

Figure 22 Pulsed DC voltage supplied to the cathode of the PVD75

When the negative dc voltage is applied to the cathode it is referred to as the "on" time (t_{on}). The "on" time is determined by the reverse time and the frequency set by the user. The reverse time (t_{rev}), as labeled in Figure 22, is the duration of time that the polarity of the voltage is reversed. The voltage is not 100% reversed, for our machine the options for the percentage of reverse polarity are 10%, 15%, and 20%. Reversing the voltage during the reverse time allows the target to be discharged and when the parameters are optimized for the process, prevents arcing from occurring. Limiting or eliminating arcs altogether is important because arcing contributes to particulate formation, which if embedded in a thin film will cause uniformity problems, and can damage the power supply [32,33] The parameters and their settings used in this research will be explained in detail in the following section.

Pulsed dc magnetron sputtering was chosen for its benefits over other processes. RF sputtering is usually used when sputtering dielectrics due to the charge build-up and hence arcing issues. RF sputtering has the drawback of low deposition rates. Pulsed dc

magnetron sputtering has the benefit of arc suppression and increased deposition rates as compared to RF sputtering and ion beam deposition which have low deposition rates. Due to the increased ionization from the magnetron the sputtering rate is increased, thereby increasing the deposition rate as well. Using a reactive process is also possible with this sputtering process as opposed to ion beam deposition or e-beam deposition. In short, pulsed dc magnetron sputtering is employed in this research due to its increased deposition rates, arc suppression capabilities and the ability to use a reactive process when sputtering.

4.3 PVD75 Description

The PVD75 is a physical vapor deposition machine that is produced by the Kurt J. Lesker Company. A picture of the PVD75 used for this investigation is shown on the following page in Figure 23.

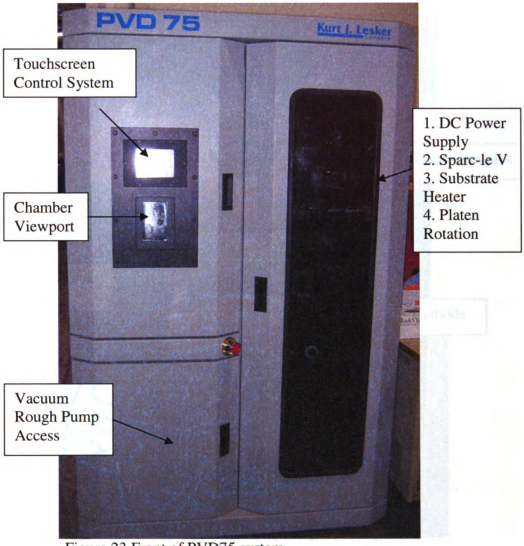

Figure 23 Front of PVD75 system

As can be seen, there is a touch screen and a chamber viewing window located in the chamber door, below this door is the door to access the vacuum roughing pump. On the right hand side is the door to access such parameter controls as the dc power supply (MDX 1.5 kW), arc suppression (Sparc-le V; frequency, reverse time, reverse voltage, etc.), the substrate heater (M.A.P.S Power Supply) and the substrate (platen) rotation.

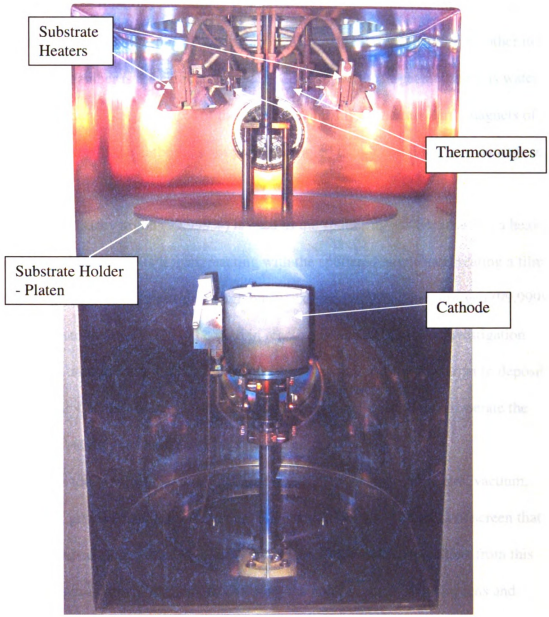

Figure 24 PVD75 Chamber

Figure 24 shows the inside of the chamber. As can be seen, the chamber has a "D-shaped" volume. The heaters can heat the substrate to a maximum of 350° C for a time of 4 – 6 hrs. The thermocouples are located next to the heaters. The platen or substrate holder can be a distance of 15 cm from the target or 7.5 cm from the target. For this research, it is a distance of 7.5 cm from the target. The platen rotation speed ranges from 0-10. There are no units for the rotation speed, but as is mentioned later in this chapter at

a speed of 5 the rotations per minute is approximately 41, so the assumption would be that at a speed of 10 the rpms would be about 82, double the speed at 5. The other item within the chamber is the cathode. The cathode is where the target sits and it is water cooled in order to keep the heat of the target transferring to the rare earth magnets of the TORUS source. If the cathode is not properly cooled then it could result in damage to the magnets.

High purity argon (99.999%) is used as the sputtering gas because it is a heavy, inert gas, which prevents it from reacting with the sputtered atoms and creating a film with a high amount of impurities. High purity oxygen (99.99%) and nitrogen (99.999%) are connected to the PVD75 to be used in reactive processes. For this investigation nitrogen is used to react with the aluminum atoms sputtered from the target to deposit as a film of AlN on the substrate. Nitrogen, not high purity, is also used to operate the pneumatic valves and shutter and for system venting.

The touch screen has four different screens for the operator to use; vacuum, deposition, gas and maintenance screen. The vacuum screen is the default screen that comes on when the machine is initially turned on. The possible operations from this screen are pump down, vent, abort, changing the color scheme of the screens and switching to one of the other 3 screens (maintenance, deposition and gas). The vacuum screen is shown on the next page in Figure 25. Upon initial start-up of the PVD the vacuum screen is the default screen.

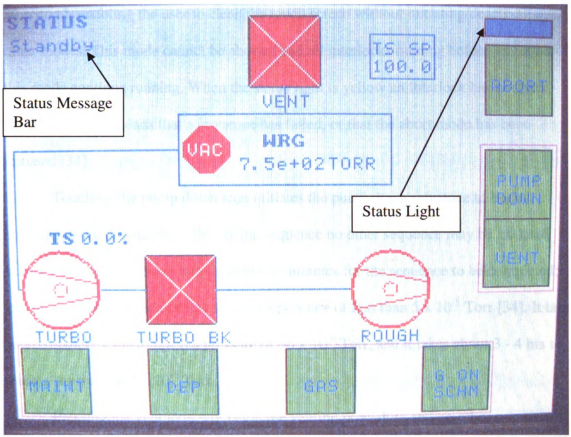

Figure 25 Vacuum screen

The items that aren't labeled already (on the screen), or for which their function/purpose is unclear to the user I have labeled, in Figure 25, and all icons are explained in detail.

The status message bar displays the individual steps in a sequence as they are being executed and interlock information when they have not been satisfied. When a sequence has been initiated the message bar displays the current step in that sequence. When an interlock has not been satisfied the message bar displays the interlock information.

The status light informs the user of the mode the machine is in by the color of the bar. If the bar is green, this represents standby mode. When the status light is blue the machine is in clean mode or a sequence is running. When clean mode has been initiated, (from the maintenance screen) all operations through the touch screen will be disabled for

30 seconds enabling the user to clean the touch screen without initiating/deactivating other modes. This mode cannot be aborted and all interlocks running before initiation of this mode continue running. When the status light is yellow an interlock has not been satisfied and red means that a sequence has failed, or that the abort mode has been initiated [34].

Touching the pump down icon initiates the pump down sequence to begin pumping down the machine. During the sequence no other sequence may be initiated except the abort sequence. It takes about 10 minutes for the sequence to be completed; this means that the machine has reached a pressure of less than 5×10^{-5} Torr [34]. It takes approximately 2 hrs to reach a pressure of $\sim 6 \times 10^{-6}$ Torr, and it takes about 3 - 4 hrs to reach a pressure of 2×10^{-6} Torr.

Pressing the vent icon will begin the venting procedure and no other sequence may be activated during this mode of operation. It takes approximately 5 minutes for the PVD75 to reach atmospheric pressure. After atmospheric pressure has been reached the chamber door may be opened and closed.

When the WRG pressure display is touched, the pressure will be displayed in bar on all screens, if the pressure was displayed in Torr prior to being touched. If the pressure was displayed in bar, prior to being pressed, it will be displayed in Torr. This icon is left in Torr to avoid confusion caused by switching between the two pressure units.

The abort mode is accessible from every screen. However, the abort mode is disabled when the screen clean mode is enabled. Pressing this icon on the touch screen will initiate a series of steps including closing the vent, rough, throttle and gas valves off, turn off the turbo molecular vacuum pump, set MFC (mass flow controller) mode to 0

and the MFC flow to 0%, the pressure set point is set to 0 Torr (or bar) and any sequence running is deactivated [34]. After this sequence of steps has finished running the PVD returns to standby mode.

In the G ON SCH mode the icon colors are green and red. Green represents on or open and red represents off or closed. Touching this icon will switch the color scheme to the R ON SCH. In the R ON SCH the icon colors are blue and red. Blue represents off or closed and red represents on or open.

Provided the pump down and vent sequences are not running and the clean screen mode has not been activated, any of the other three screens may be accessed. Normally, the next screen selected is the gas screen.

Pressing the gas icon will switch the user to the gas screen shown in Figure 26.

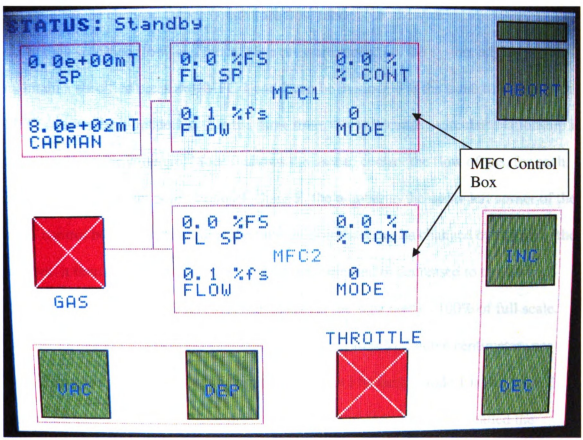

Figure 26 Gas screen

From the gas screen the user can set the pressure at which to sputter the film, the mode to run the MFC's and switch to the vacuum or deposition screen. There are two mass flow controllers (MFC) labeled MFC1 and MFC2. For this investigation, MFC2 is the sputtering gas, high purity Ar (99.999%), and MFC1 is connected to high purity nitrogen (99.999%) and oxygen (99.99%) for use in reactive processing. The high purity oxygen has not been used (at this time) for processing; only high purity nitrogen is used for this research to deposit an AlN film.

There are 3 modes to run each MFC and they are labeled 0, 1 and 2. The mode can be changed by touching the number labeled mode. It will become highlighted and can be changed using the INC/DEC icons. If the INC/DEC buttons are not touched for 5 seconds the number will be un-highlighted and must be touched (highlighted) again before it can be changed. Mode 0 and 1 are flow modes (i.e. the system adjusts to maintain a specified flow) and mode 2 is a pressure mode (i.e. the system adjusts to maintain a specified pressure). MFC 1 and 2 can be in mode 0 at the same time, but both MFC's cannot be in mode 1 or 2 at the same time; this is because a circular relationship is not allowed by the software. Mode 0 allows the user to control the flow of gas, for each channel, by using a set point. For each channel, the number in the upper left corner of the MFC control box marked FL SP is the flow set point and can be changed by touching the number, it then becomes highlighted and can be increased or decreased to the desired flow using the INC or DEC icons. Valid inputs for the flow are 0 – 100% of full scale. For the nitrogen processing gas full scale is 100 sccm (standard cubic centimeters per minute) and for the argon processing gas full scale is 139 sccm. Mode 1 is the "slave" mode; this means that the MFC in mode 1 is "slaved" to the other MFC (called the

"master"), which must be set to mode 0 or mode 2. The MFC set to be in mode 1 will flow a percentage of the flow rate set for the master MFC and the throttle valve will adjust the pressure as needed. This percentage is the contribution percent labeled % CONT and located in the upper right hand corner of the MFC Control Box, in Figure 23. To set this percentage touch the % CONT number to highlight it and using the INC/DEC icons set the contribution to the desired percentage. For example, if MFC1 is flowing 40% of full scale and MFC2 is slaved to it with a percent contribution of 50%, then MFC2 will flow 20% of full scale. Mode 2 is a pressure mode. In mode 2, the desired deposition pressure is set by the user and values from 0 – 1000 mTorr are valid. Touching the number labeled SP, in the upper left hand corner of the touch screen, will highlight it and then set the chamber pressure to the desired pressure. Now the total gas flow adjusts to maintain a set pressure and the slave MFC will contribute a percentage of the flow of the master MFC.

When all the desired flows and or pressures are set touch the GAS valve icon to turn the output on (it will be green in color when it is on) and allow gas to flow to the chamber, then touch the THROTTLE valve icon to turn its output on (it will be green when it is on); this valve helps control the pressure in the chamber. After the pressure is set and the number (labeled SP) is no longer highlighted the software will automatically adjust the flow rate of the MFC until the pressure reaches the set point. The actual pressure of the chamber is shown just below the set point with the number labeled CAPMAN and the actual flow of the MFC is the number in the lower left hand corner of the MFC control box labeled FLOW.

To switch to the deposition screen touch the icon labeled DEP. The deposition screen is shown below in Figure 27.

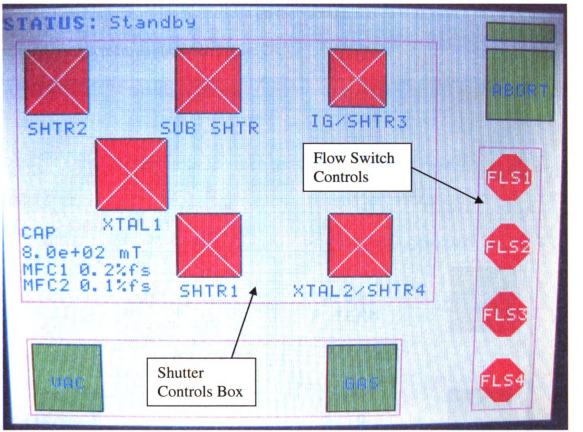

Figure 27 Deposition screen

The screen in Figure 27 shows the shutter controls and the flow switch indicators for the deposition screen. The PVD75 (for this research) is equipped for sputtering only and has one sputtering gun, therefore the icon labeled SHTR1 (shutter 1) is the only shutter used. Touch the icon to open or close the shutter, it will be green when the shutter is open and red when the shutter is closed. However, for this investigation, because the platen has been modified to be closer to the target the shutter has been removed because it would not open entirely if it were attached to the cathode. The flow switch controls indicate whether or not the flow set point for the MFC has been satisfied, it is green if it is satisfied and red if it is not. The numbers in the lower left hand corner of the shutter

controls box are as follows; the number labeled CAP is the actual pressure of the chamber, MFC1 is the actual flow of MFC1 and MFC2 is the actual flow of MFC2.

Touching the maintenance icon on the vacuum screen will switch the user to the maintenance screen, as shown in Figure 28.

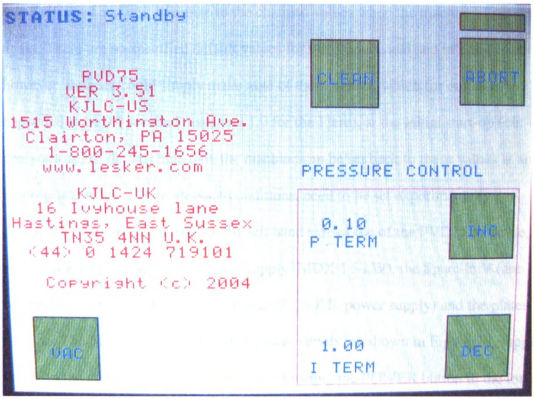

Figure 28 Maintenance screen

From this screen Kurt J. Lesker's contact information is available making it convenient to reach them while you are still near the PVD75 when there is a problem. Depressing the icon labeled clean on the touch screen will initiate the clean mode.

The pressure control icons are for manually setting the proportional and integral terms (PID pressure control parameters). These terms may need to be adjusted for the pressure control loop to function properly and cannot be adjusted while the pressure control loop is running. The pressure control loop is the program/software that adjusts the flow of the gas to attain the pressure set point when the MFC is in mode 2. By touching

the term to be changed, it will be highlighted and using the INC/DEC icons to the right of the screen allows the user to increase or decrease the term to the desired set point. Acceptable values for these terms are 0 – 99.99. If the INC/DEC square is not pressed within 5 second the term chosen will no longer be highlighted. These terms are saved when changed and will initialize to the changed values when the machine is powered up again. There are no specified default values for the proportional and integral controls, however, the user could simply make note of these values, which for our machine happened to be 0.1 for the P term and 1.0 for the I term, at the initial start-up (out-of-the-box start-up) of the machine then the machine can be set back to these values at any time. Appropriate values, for processing conditions, need to be set experimentally.

The parameter controls on the left hand side of the of the PVD75 machine, as shown in Figure 23, are the dc power supply (MDX 1.5 kW), the Sparc-le V (arc suppression controls), the substrate heater (M.A.P.S. power supply) and the platen rotation. The MDX 1.5 kW magnetron power supply, as shown in Figure 29, supplies power to the cathode of the sputtering gun. Pushing the POWER button in the lower left hand corner of the MDX will turn it on.

Figure 29 MDX 1.5 kW magnetron drive

The magnetron drive has the option of supplying output in the form of power, current or voltage regulation. These buttons are located under the label REGULATION in Figure 29. Pressing the buttons marked power or current will regulate the output with these parameters. If both the power and the current button are pressed at the same time the output will be regulated by voltage. The regulation mode cannot be changed when the output has been turned on, the lights will go on or off when pressed but the mode will not change when the output is on [35]. The power output range is from 0 – 1500 W, the voltage output range is from 0 – 750 V, and the current output range is from 0 – 2 A. The actual output, based on what is chosen, is displayed to the right of the Actual Output label. For this investigation, power output regulation is used.

To set the output value of the MDX press the button marked SETPT under the label RIGHT DISPLAY and then turning the knob under the LEVEL label until the desired set point is reached. If the SETPT button is pressed a second time the user can adjust the ramp time of the output by turning the knob below the RAMP ADJUST label until the desired ramp time is reached. The time for ramping the output can be set from 0 -10 either in seconds or in minutes. Pressing the ACTUAL button once, next to the SETPT button, will display the actual output power in watts, pressing it twice will show the actual output voltage in volts and pressing it a third time will show the actual output current in amps.

There are four pairs of LEDs just below the output displays (actual and set point), as shown in Figure 30; these are the LED status messages.

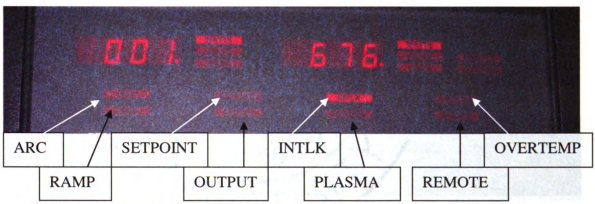

Figure 30 LED status lights on the MDX

From left to right, the ARC LED lights when an arc has been detected by the MDX and has triggered the activation of the ARC-OUT circuit. The ARC-OUT circuitry helps to suppress and quench arcing. The RAMP indicator light flashes quickly when the output is ramping toward the set point and turns off when ramping is finished. The SETPOINT light turns on when the output is within .2% of the programmed set point and flashes when the output is on and the output is not within .2% of the set point. This light turns off

when the output is turned off. The OUTPUT LED is lit when the output has been turned on. The INTLK indicator light is lit when all interlocks have been satisfied and flashes if all interlocks have not been met. The PLASMA light is lit when the output is on and the output current is greater than 2% of the maximum current available for the MDX model. The OVERTEMP lights if the MDX has overheated. The REMOTE LED lights if control of the MDX is set to remote and is controlled by computer. Once all the parameters are set the output can be turned on and off by pressing these buttons below the OUTPUT label.

The Sparc-le V pulses the dc output from the MDX and sends it through to the cathode in the chamber; it is meant to enhance the arc handling capability of the MDX power supply. Sparc-le V actually stands for Small Package Arc Repression Circuit-Low Energy Variable. The Sparc-le is shown in Figure 34 and 35. Figure 34 shows the entire Sparc-le face and Figure 35 shows only the parameter menus and the programming buttons.

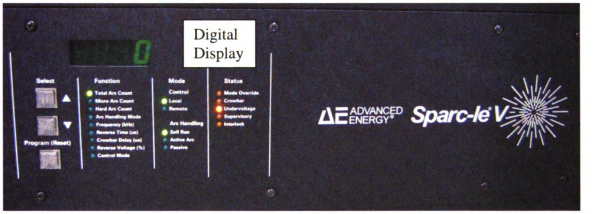

Figure 31 Sparc-le V pulsing and arc suppression device

The digital display window above the parameter settings displays the value of each setting when it is chosen (the LED in front of the parameter is lit). There are 4 menus, shown on the following page in Figure 32; the function menu, which is the main menu;

two submenus, mode control and arc handling, which can be accessed from the function menu; and a status menu, which gives the current status of the Sparc-le V. In order to access the submenus (mode control and arc handling) from the function menu, use the Select arrow keys to move the lit LED to desired submenu, push the Program button to select the submenu, the LED in front of the submenu will blink, the user can now use the Select arrow keys to choose a setting for that submenu (i.e. select either local or remote for mode control), once the setting for that submenu has been chosen push the Program button and the LED in front submenu will stop blinking and this signifies that the user can move through the function menu items.

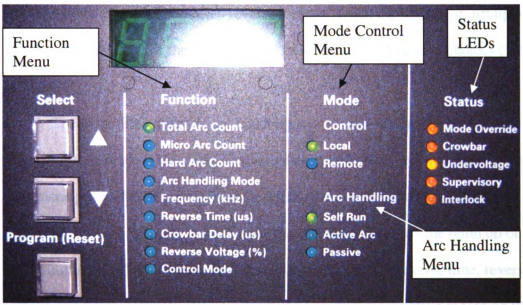

Figure 32 Sparc-le V menus and programming buttons

As mentioned above, to scroll through the menus use the up/down arrows under the Select label on the left hand side of the Sparc-le. In the function menu the first three items are arc counts (total, micro and hard), which are counted while the output of the MDX is on. These can be cleared at any time by pressing the Program (Reset) button located on the bottom left hand side of the Sparc-le. The rest of the items in the function

menu are the arc handling mode, frequency (in kHz), reverse time (in μs), crowbar delay (in μs), reverse voltage (in %) and the control mode. With the exception of the reverse voltage percent, all of these items can be changed by scrolling down to the item; push the Program (Reset) button to select the item. The light in front of the item will blink and the user now has access to that parameter or submenu. To set the parameter or the submenu setting to the desired point use the up/down arrows, when the parameter is set push the Program (Reset) button again, the LED will stop blinking and stay lit until a select button is pushed to move to the next item. Before changing the reverse voltage, be SURE that the MDX output is turned off. The reverse voltage percentage can be changed by scrolling down to the LED labeled reverse voltage. When the LED is lit, lift up on the T-handle (located on top of the Sparc-le) and move it to one of percent choices (10%, 15%, or 20%).

There are three different arc handling modes, self-run, active arc and passive mode. Self-run mode is the mode in which the Sparc-le is always operated, in this study. This mode pulses the dc power from the MDX at a user defined frequency. This pulsing, discharges any charge that has built-up in the chamber and slows the build up of an insulating film [36]. Self-run mode allows for the frequency, reverse time, reverse voltage and the crowbar (hard arc) delay to be adjusted. Information regarding the active arc and the passive modes are available in reference [36].

The frequency parameter allows the user to set the frequency at which the power from the MDX is pulsed. This frequency is shown in kilohertz (kHz) and ranges from 1 – 100 kHz. This range goes from 1 – 5 kHz in increments of 1 kHz, the frequency then

jumps from 5 kHz directly to 20 kHz. The frequency range then goes from 20 – 75 kHz in increments of 1 kHz and it goes from 75 – 100 kHz in increments of 5 kHz.

The reverse time, t_{rev}, is the amount of time that the voltage to the target is reversed in polarity (during the t_{on} the voltage is negative, thus during the t_{rev} the voltage is positive). This time is in μs (micro-seconds) and the range to choose from differs depending on the frequency that is selected. Table 4 listed below, shows the break down of the frequency ranges that match the reverse time ranges [36].

Table 4 Reverse time ranges matched to frequency ranges (from reference [36])

Frequency (kHz)	1-5, 20-50	51-55	56-60	61-65	66-70	71-75	80-100
Reverse Time (μs)	1-10	1-7	1-6	1-5	1-4	1-3	1-2

The crowbar delay is the last attempt to quench an arc. This parameter can be set to 10, 30, or 50 μs. At 10 μs, the Sparc-le tries to clear the arc once before it shorts the output of the MDX power supply. At 30 μs the Sparc-le will attempt to clear the arc twice before it shorts the output of the power supply and at 50 μs it will attempt to clear the arc three times. When the output of the power supply is shorted it is shutdown for 7 ms (long enough to clear the arc) and then the output from the MDX is reinstated and continues its normal operation.

Reverse Voltage is the percent of the initial voltage that is reversed in polarity. For example, if the t_{on} voltage (initial voltage) is set to 500 V (as mentioned previously, this voltage is negative in polarity) and the reverse voltage is set to 10%, then the reverse voltage will be 50 V (of positive polarity). The reverse voltage can be set to 10, 15, or 20%.

There are two different control modes at which to set the Sparc-le V, they are local and remote. For this investigation the Sparc-le is always set to local mode; this means that the Sparc-le parameters are adjusted from the front of the Sparc-le (they are set manually). If the Sparc-le is in remote mode then the parameters are adjusted remotely from the rear of the machine via the user port or the host port.

The status menu, located on the far right in Figure 32, shows the status of the Sparc-le V. The status LEDs are labeled as follows, mode override, crowbar, under-voltage, supervisory and interlock. The mode override LED in the status menu will light when there are any one of the following faults detected, input over-current, over-temperature, over input power, over-voltage, line voltage fault, tap select interlock fault, switch over-current, slave fault, slave error, or processor error. When one of these errors occurs the Sparc-le V is disabled, but the power to the load is not interrupted. This is an undesirable situation because there is neither arc suppression nor a reverse recovery. If this situation occurs, system troubleshooting is necessary. After the condition has cleared the Sparc-le V will turn on again automatically to the same mode prior to being disabled. The LED will remain lit until the fault has been cleared by pressing the program (reset) button twice [36]. When a mode override error occurs an error code will display for 1 s and a normal display resumes. The error code will redisplay by pressing any button on the Sparc-le V. If multiple errors occur only the last error code will display. For convenience, the table of error codes, Table 5 shown on the following page is copied from reference [36].

Table 5 Sparc-le V error codes and their meanings, taken from reference [36]

Error Code	Description
E01	This is an over-voltage error. The active arc and self-run switches are disabled for 1 ms but power is not interrupted from the MDX to the chamber.
E02	This is an input over-current error code. The crowbar is initiated to short the dc input power to the Sparc-le.
E03	This is an over-temperature error code. The Sparc-le is disabled and the passive mode is enabled until the unit cools down. The error code display remains until the unit has cooled.
E04	An over input power has occurred, which means the power has exceeded 12.5 kW. The active arc and self-run switches are disabled until the fault is cleared.
E05	This is a line voltage fault. When this error occurs the active arc and self-run modes are disabled for 100 ms.
E06	A tap select interlock fault, this means that the T-handle to adjust the reverse voltage is up. The active arc and self-run modes are disabled for 100 ms while the handle is raised. This interlock fault could also mean that the ARC-OUT enhancement relay drive has malfunctioned and the Sparc-le requires repair service.
E07	This indicates a switch over-current, at which time the reverse time is shortened until the error clears
E08	This is a slave fault and it means there is one of the following errors in the slave Sparc-le, over-temperature, line voltage input, over input power, switch over-current, or over-voltage. (Note: for this research we do not have multiple Sparc-le's set up in the master/slave orientation)
E09	Slave error means that the slave has lost line voltage or the master/slave cable is bad. (Note: for this research we do not have multiple Sparc-le's set up in the master/slave orientation)
E10	This indicates a processor error (internal) or power has been lost to the user port and requires a manual startup.

The crowbar status LED will flash for 5 ms each time a crowbar event occurs. The under-voltage will light when the dc input voltage is lower than 150V. When the supervisory LED is lit (continuously) this means that the Sparc-le V has an internal malfunction. The LED sometimes blinks during hard arcing but it only indicates a problem when it is continuously lit. When the interlock light is lit when the back cover on

the output connector is off or the T-handle for the reverse voltage is not seated properly [36].

The M. A. P. S. heater power supply is the power supply that controls substrate heating. It also monitors the temperature of the substrate. The substrate heater is shown in Figure 33.

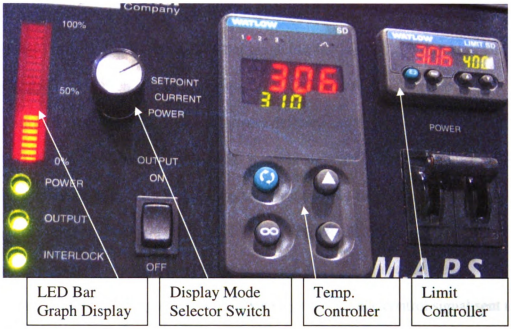

Figure 33 M.A.P.S. Heater Power Supply (substrate heater)

To turn on the heater power supply on flip the switch, under the POWER label in the lower right hand corner of Figure 33, to the up position. To turn off the heater power supply, flip the switch to the down position. This switch also acts as overall current protection as well.

The LEDs in the lower left hand corner are the power, output and interlock indicators. When all interlocks are satisfied the LED labeled INTERLOCK will be lit. When power to the heater power supply has been switched on the LED labeled POWER will be lit. When output from the heater has been turned on the OUTPUT LED will be lit.

To turn on the output from the heater power supply to the quartz lamps in the chamber, push the ON portion of the switch under the label OUTPUT. Once it is pushed the output LED will light and stay lit. Pushing the OFF portion of the OUTPUT switch turns the output LED off and output to the quartz lamps is shut off. When the ON or OFF switch is pushed it will not stay locked in place, it will return to the neutral position.

The LED bar graph display, labeled in Figure 33, has markings of 0, 50 and 100 % to the right of the bar graph display. The bar graph display has 20 LED bars total and is linearly scaled so that each bar represents 0.5 V_{DC} of the control signal to the SCR (silicon controlled rectifier), which controls power delivery and has a 0 – 10 V_{DC} signal range [37]. It should be noted that the set point is not linear with the applied voltage.

The display mode selector switch selects the function of the bar graph display. There are three settings which are labeled, SETPOINT, CURRENT and POWER. The current and power selections are non-functional and are there for future use (i.e. upgrades). The setpoint setting gives the user a visual of the voltage control signal sent to the SCR.

The temperature controller, as labeled in Figure 33, allows the user to set the desired temperature. The temperature controller allows the user to program, heating processes into the device, which allows for plethora of variables to be set for strict control over the heating process. For further information on how change specific variables and/or program the temperature controller please see reference [38]. Our process is simple and does not need such explicit control. The temperature is set to the desired set point and allowed to ramp up to temperature, before the plasma is ignited. The substrate is kept at this temperature for the entire deposition process. To set the temperature, push the

up/down arrow at the bottom right hand side of the temperature controller until the desired temperature is set. The set point is in small yellow numbers in the second row of the digital display. The actual temperature (as measured by the thermocouples in the chamber) is in large red numerals in the first row of the display. There are three process LEDs, labeled 1, 2 and 3 in the upper left hand corner of the temperature controller. When the temperature is set manually, as just described, the LED labeled 1 will blink until the set point has been reached.

The limit controller, in the upper right hand corner of Figure 33, is used to prevent process conditions from going out of control limits and damaging the substrate and or chamber parts. The limit controller allows for many different parameters to be set by the user, but our process is a simple one and only the over-temperature is set. For more information on parameters that can be set and how to program the limit controller please see reference [39]. To set the temperature limit, use the up/down arrow keys located in the bottom right hand corner of the limit controller until the desired absolute maximum process temperature is set. The set point is in small yellow numerals on the far right of the digital display. The actual temperature, as measured by the thermocouples in the chamber, is in large red numbers on the left of the display.

The last of the parameter controls for the PVD75 is the platen (substrate) rotation control, shown in Figure 34.

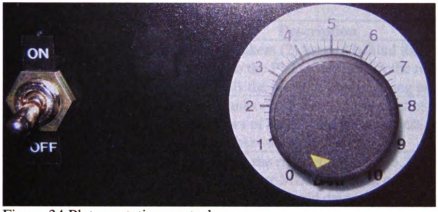

Figure 34 Platen rotation control

To turn the platen rotation on, flip the toggle switch on the left hand side of Figure 31 to the ON position. To turn the platen rotation off, flip the toggle switch to the OFF position. Before turning the rotation on the rotary knob should always be set to 0. Turn the rotation on and slowly adjust the knob to the desired speed. The rotation speed setting can range from 0 – 10. Based on experience, if the speed is set above 5 the rotation can become unstable and cease to rotate; therefore the rotation speed is never set higher than 5. At a setting of 5 the rotations per minute (rpm) is 41. At the time this thesis was written, the rotation would cease when the plasma was turned on. The source of this problem has yet to be ascertained.

4.4 PVD75 Operating Procedures

To begin working with the PVD75, one must go through the start-up procedure to turn on the machine; the steps are listed on the following page in Table 6.

Table 6 PVD75 Start-Up Procedure

Steps	Description
1	Turn on the main circuit breakers (2) located behind the machine. The breaker on the left controls power to the PVD75 except for the roughing pump. The breaker on the right controls the power to the roughing pump
2	Turn on the nitrogen gas tanks (2), located to the right of the PVD75 in the center row. There are 3 rows of tanks. One tank controls the valves and sputtering shield and the other vents the chamber.
3	Turn on the chiller located to the right of the PVD75. Be sure the chiller is set to 20 °C once it is on. The chiller MUST be on in order to operate the PVD75. (Note: If it is below 20 °C on hot humid days condensation will build up on the machine creating an electrical hazard)
4	Turn on the power-box circuit breaker, located inside the left rear panel at the top of the machine, as shown in Figure 35. The green LED located above this switch will be lit when the switch is in the ON position
5	Turn on the power switch to the MDX 1.5 and the Sparc-le V (located on the back of the respective devices) accessible from the rear of the PVD75.

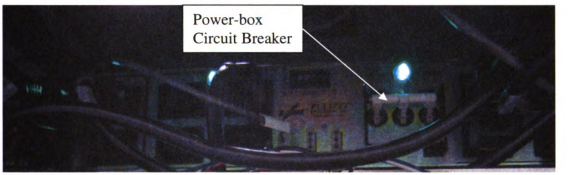

Figure 35 PVD75 Power-box

Now that the PVD75 is on, affix the substrate to the platen and place it back into the chamber. Wipe down the chamber walls using IPA (isopropyl alcohol, to avoid leaving a residue when it evaporates, as with acetone, or methanol) and target to remove any loose and unwanted particulates, a source of arcing. This should be done before or after every run. Check the target to ensure that the proper target has been installed, for target removal and installation instructions please refer to reference [40]. Close the chamber door and begin the pump down procedure as described previously. Wait until the pressure is at least 4×10^{-6} Torr before beginning the deposition procedure.

After the pump down procedure has finished the parameters can now be set for the deposition process. The process used to deposit the AlN layer is a reactive process; for this investigation it means that a target of Al was sputtered in a nitrogen gas enriched environment and combined with the nitrogen before depositing on the substrate as a layer of AlN. Listed in Table 7 is a description of the deposition procedure.

Table 7 AlN Deposition procedure

Steps	Description
1	Set the substrate temperature and turn on the heater output. Allow approximately 15 – 30 minutes for the temperature to reach its set point.
2	Turn on the high purity nitrogen and argon gases.
3	Set the deposition chamber pressure from the gas screen on the PVD75.
4	Set the mode for each gas (nitrogen and argon) and the parameters related to each mode.
5	Turn on the gas and throttle valves.
6	Set the parameters on the Sparc-le V.
7	Set the parameters for the MDX.
8	Turn on the output from the MDX for the specified time.
9	When the deposition time is reached, turn off the output to the MDX.
10	Turn off the substrate heater and allow to the platen to cool overnight before removing the substrate from the chamber.

In Tables 8 – 10 are listed the parameter settings used to deposit AlN onto ultrananocrystalline diamond (UNCD). The frequency of 50 kHz and a reverse time range of 3 - 5 μs were chosen because for the AlN reactive process this was the frequency and reverse times at which arcing was minimal and made for a more stable process for the duration of the run time. The crowbar delay is set at 10 μs so that the Sparc-le will try to clear the arc once and then will cut-off power from the MDX to quench the arc. Arcing causes unwanted effects to the deposited layer and at worst it could do damage to the MDX power supply. The control mode is always set at local so the Sparc-le can be controlled from the front panel.

Table 8 AlN Parameters for the Sparc-le V unit in the PVD75

	Arc Handling	Frequency	Reverse Time	Crowbar Delay	Reverse Voltage	Control Mode	Substrate Rotation
Sparc-le V	Self Run	50 kHz	3 - 5 µs	10 µs	10 %	Local	0

Table 9 shows the parameter settings of the MDX power supply. The power was set to the maximum power that could be output given the Sparc-le settings.

Table 9 AlN Parameters for the MDX 1.5 kW

	Power (Constant Power Mode)	Ramp Time
MDX 1.5 kW (Power Source)	450 - 375 W	7 s

Table 10 shows the chamber pressure settings used for the AlN deposition. As previously noted, the base pressure (pressure the chamber is initially pumped down to) is pumped down to at least 4 x 10^{-6} Torr to have minimal impurities in the chamber at the time of deposition. The rest of the chamber parameters were set based on previous works [20,21,23,30,32,41,42].

Table 10 AlN Parameters for inside the chamber of the PVD75

	Base Pressure	Deposition Pressure	Gas Flow (Argon ; Nitrogen)	Substrate Temperature	Substrate Distance to Target
Chamber	$< 4*10^{-6}$ Torr	3 mTorr	Mode 1 ; Mode 2 33.3% cont. ;	350 °C	~ 7.5 cm

Table 11, shown on the following page, explains the steps of the shut-down procedure for the PVD75.

Table 11 PVD75 Shut-down procedure

Steps	Description
1	Turn off the power button on the front of the MDX.
2	Turn off the gas valve and the throttle valve on the gas screen.
3	Shut off gas flow from the high purity nitrogen and argon tanks (on the tanks).
4	Switch to the vacuum screen, vent the chamber, wait for the chamber to reach atmospheric pressure and wait for the status message bar be in stand-by mode.
5	Turn off the power switch to the MDX 1.5 and the Sparc-le V (located on the back of the respective devices) accessible from the rear of the PVD75.
6	Turn off the power-box circuit breaker, located inside the left rear panel at the top of the machine, as shown in Figure 35. The green LED located above this switch will turn off when the switch is in the OFF position.
7	Turn off the the main circuit breakers (2) located behind the machine
8	Turn off the nitrogen gas tanks (2), located in the center row
9	Allow the chiller to remain on for at least 15 minutes to avoid damaging the magnetrons and then turn the chiller off.

Some expectations for a typical run would be that the power would stay within 20% of its set-point. The reason for this large percentage is because as the process runs the chamber conditions change and the target degrades as well, which causes the actual power output to fluctuate and decrease as the power output is on. Even from run to run the power cannot always be set to the initial start value of the previous run due to this phenomena and it is sometimes difficult to gauge where the power needs to be set upon start-up in order to achieve optimal results (i.e. high deposition rate, uniformity, etc.). It would also be expected for a typical run that upon ignition of the plasma there is a high amount of arc activity, usually this spike occurs within the first 30 – 60 seconds of igniting the plasma (turning on the power output). This spike in arc activity can be minimized by adjusting chamber parameters, but at the cost of deposition rate. This initial spike in arcing could be due to build-up of insulative material from the previous run, redeposition of material on the target, flakes, or particulates on the target. The target can

be "scrubbed", a pre-clean of the target with the shutter closed to specifically rid the target of most of these issues, prior to deposition for 10 – 15 minutes. However, the target cannot be "scrubbed" during the AlN deposition due to the platen distance from the target. The shutter is has been removed because the distance from the platen to the target would hinder it from opening all the way. If it was left on it would not only damage the substrate/sample, it would partially block the plasma from getting to the substrate as well. An average of 150 arcs or less is appropriate upon plasma ignition. Also an average of 250 arcs or less is expected for total arcs for an entire run. This is of course dependent on the expectations for the layer upon completion, if the uniformity does not matter (e.g. it is a sacrificial or masking layer) than more arcs than this may acceptable. As for hard arcs, no matter what the situation an average of 1 or 2 is acceptable for an entire run, but the absolute maximum would be 5 (and only upon initial start-up, because it is over a short duration of time, between 30 and 60 seconds, as mentioned above), any more than this and the system would need to be shut down and the cause would need to be found and eliminated. The expectations for the completed layer would determine whether or not the platen rotation would need to be on or off. In this research for a typical AlN run the rotation is off. For an average run it would also be expected to be an error free run, i.e. none of the errors described in Table 5 would be experienced.

Chapter 5

Aluminum Nitride Deposition Observations

5.1 Introduction

This chapter will discuss the observations made after deposition. First, a discussion of general observations are made, such as measurements concerning surface roughness, substrates used and deposition parameters. Next, characteristics of the film that will be discussed are growth rate, uniformity and adhesion. Optical data, transmission and reflection, were also collected. Then, x-ray diffraction (XRD) was used to determine the chemical composition and lattice structure of the deposited layer. Finally, scanning electron microscopy (SEM) was used to determine grain growth.

5.2 Deposition Observations

Aluminum nitride was deposited on different surfaces, glass (microscope slides), silicon and UNCD. A list of all samples for this thesis is included in Appendix A. The initial (trial) runs were done on glass microscope slides; these are called trial runs because this was the initial phase of using the PVD75 and involved becoming familiar with the parameters. These runs were with a non- heated substrate and performed under arc-less conditions under the assumption that arcing causes undesirable effects to the deposited film layer. However, under these arc-less conditions we were unable to take advantage of the higher deposition rates by using pulsed dc magnetron sputtering. For some of the later samples, on silicon substrates, the substrate was heated. As noted

previously, the deposition parameters for these samples are listed in Tables 8 – 10. A shortened list is shown below in Table 12.

Table 12 Shortened list of AlN deposition parameters

Parameter	Value
Pressure	3 mTorr
Frequency	50 kHz
T_{rev}	3 μs
N_2: Ar	3:1
$Temp_{substrate}$	350 °C
Power	370 – 450 W

The samples with AlN deposited onto Si were observed to be smooth and transparent. Measurements with a Dektak were shown to have R_a values in the range of 0.6 to 2 nm and R_z values in the range of 10 to 50 nm for scan lengths of 1- 2 mm. A representative sample, CF-018, had an R_a value of 0.78 nm and an R_z value of 28.77 nm and a thickness of 800 nm. Some samples (using glass and silicon substrates) and their parameters are listed below in Table 13.

Table 13 Samples of AlN and some of their parameters

Sample	Deposition Time	Distance to Target	Rotation	Thickness	Deposition Rate	Young's Modulus
CF-008	120 (min)	15 (cm)	Yes	120 (nm)	60 (nm/hr)	150 (GPa)
CF-009	120	7.5	No	300	150	x
CF-016	64	7.5	No	493	462	280
CF-017	163	7.5	No	1500	551	330
CF-018	120	7.5	No	800	400	353
CF-019	35	7.5	No	187	322	x

The Young's modulus was also lower on the sample run with a distance to the target of 15 cm as opposed to the samples that ran at a distance of 7.5 cm to the target. Optical data was taken for sample CF-018 to confirm the thickness of the AlN layer. A thickness of approximately 1267 nm was found using this method and the thickness found using the Dektak profilometer was 800 nm, as listed in Table 13. A possible reason

for this discrepancy is that the AlN layer was deposited without platen rotation, which means that due to the non-uniformity of the plasma (characteristic race-track formation) the deposited layer will be non-uniform as well. If the rotation were turned on then the deposited layer would be more uniform. Another possible reason for the discrepancy is that when using the profilometer to assess the thickness of a sample a precise step is needed not a gradual slope. A method for getting a crisp step was not found and used until the last sample (CF-022) was run in the PVD75.

5.3 Deposition Rate

The growth rate of the film is dependent on the parameters set on the Sparc-le V and the chamber parameters. These parameters affect the maximum setting, i.e. the power/voltage/current setting that the MDX can output. For this investigation the power was used as the setpoint for the MDX output. Once the current of the MDX reaches 2 A then this is the upper limit of the power output from the MDX.

As mentioned in a previous chapter, the settings on the Sparc-le V are as follows; arc handling mode, frequency (in kHz), reverse time (in μs), crowbar delay (in μs), reverse voltage (in %) and the control mode. The settings that were adjusted for this investigation are the frequency and reverse time. It was found experimentally that the frequency had the most effect on minimizing arcs and that the reverse time had the largest effect on maximizing the possible output voltage from the MDX power supply. The effect on the MDX output is important because the more power there is the higher the deposition rate. This means that any parameter that has an effect on the output of the power supply will cause the deposition rate to be effected as well. The reverse time range depends on the frequency setting, the higher the frequency the lower the possible

setting of the reverse time. These times and frequency ranges are listed in Table 4, Chapter 4, but in general the reverse time could possibly be set from 1-10 μs. The higher the setting of the reverse time means that the maximum output of the power supply is lower and thus causing the deposition time to be lower. For example, the earlier "test" runs for the PVD75, that were done on glass microscope slides, were run for approximately one hour with the reverse times set to 10 μs (in order to deposit under arc-less conditions) and the layer thickness for some of these runs are listed in Table 14 below. In comparison to some of the later runs (which are listed in Table 13), it can be seen that changing the reverse time makes a big difference in deposition. For example, the deposition time for sample CF-018 was 2 hours, which corresponds to a deposition rate of 400 nm/hr.

Table 14 Sample deposition rates

Sample #	Deposition Rate (nm/hr)	Deposition Time (min)	Reverse Time (μs)	Thickness (nm)	Distance to Target (cm)
CF-001	70.2	65	10	76	15
CF-002	57	60	10	57	15
CF-003	62	60	10	62	15
CF-004	40	60	10	40	15

The trial samples, on glass, which were run under arc-less conditions and at a distance of 15 cm from the target had low deposition rates. Those samples (on silicon substrates) that were run at a distance of approximately 7.5 cm from the target had higher deposition rates. As can be seen from sample CF-009 above, simply by making the distance to the target smaller the deposition rate was over triple what sample CF-004 was and slightly larger than double the deposition rate for sample CF-001.

Another parameter that also has an affect on the deposition rate is the wear of the target over time. As the target is used, the maximum power level that can be attained decreases; sometimes it can even be seen within the same run, if the run is long enough. For example, sample CF-019 was run for 2 hrs and the power was set to 420 W. The setpoint was attained initially, but by the end of the run the power level had decreased to 364 W. No measurements were made for this effect due to the nature of the deposition process. A systematic study was not performed to determine how this variation in power levels during deposition affects the deposition rate. It can be said that the deposition rate decreases but by how much exactly cannot be said, based on the data collected to date.

5.4 Uniformity

For this investigation, achieving a uniform AlN film was not a high priority. All that was necessary for this research was creating a piezoelectric film of AlN with a (002) orientation. However, for future work and for the layer of Al needed to create the electrodes of the SAW devices a uniform layer is necessary. The parameters that have an effect on uniformity are, target erosion/wear, distance to target from the substrate, substrate rotation and the position of the substrate over the target. Each of these parameters affects the others, in other words they are not independent from each other.

As a target is used it erodes unevenly in a "racetrack" shape around the target, as shown below in Figure 36.

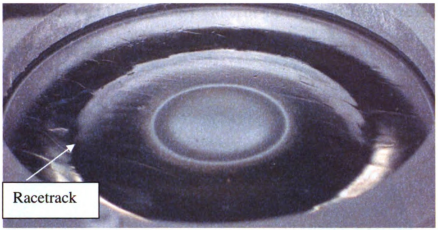

Figure 36 Racetrack erosion of used target

This racetrack erosion is caused by the design of the magnetron. This erosion pattern leads to a non-uniform plasma and this in turn leads to a non-uniform deposition layer. If, however, the substrate is rotating this aids in achieving a uniform coating. The other two parameters that also help in getting a uniform layer are distance to target and the placement of the substrate over the target (plasma). If the distance to the target is small then the placement of the substrate is crucial, the entire wafer must be placed as directly over the plasma as possible. The substrate must also be rotated in order to get a uniform deposition layer. Figures 37, 38, and 39, show photographs of samples CF-019, CF-008 and CF-009, respectively. Sample CF-019 had no rotation and was a distance of ~7.5 cm to the target and it was placed directly over the target plasma for deposition. The sample thickness is phi-symmetric, decreasing radially from the center. Sample CF-008 was a distance ~15 cm from the target with rotation and was not placed directly over the target. Although, the entire wafer is not shown in Figure 38 due to sectioning it for XRD and other analysis, the entire wafer was uniformly coated. Sample CF-009 was a distance of ~7.5 cm from the target and was placed slightly off-center from the target and the

deposition was done with no rotation of the substrate. Under these conditions the thickness is not phi-symmetric.

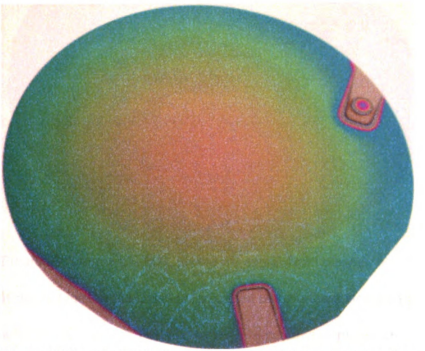

Figure 37 Sample CF-019, ~7.5 cm above the target, no rotation

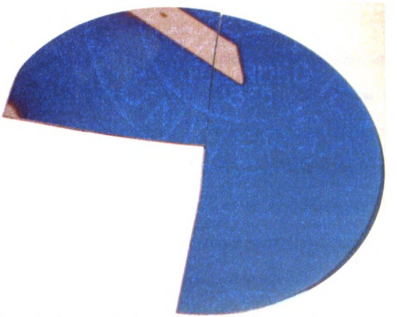

Figure 38 Sample CF-008, uniformly coated sample, with rotation

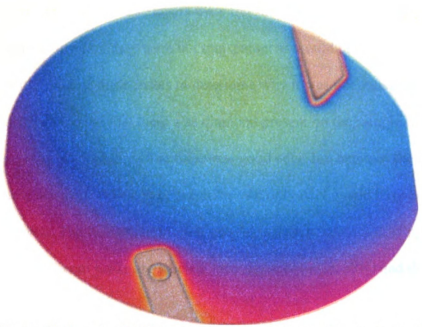

Figure 39 Sample CF-009, placed off center from plasma, no rotation

If the distance to the target is large then the sputtered atoms have a greater distance over which to spread out. This allows for a larger area of placement of the substrate on the platen and still leaves the possibility of achieving a uniform coating of the substrate.

5.5 Adhesion

The adhesion for all the samples was tested using a tape test. All of the samples had excellent adhesion to the substrate. Sample CF-022 was found to have good adhesion to the diamond interlayer; this was found using two different methods. The first method was the tape test and the second method was XRD. XRD is not a method of determining adhesion, but due to the circumstances we were able to use it to determine that the adhesion between the UNCD interlayer and the AlN layer was good. The sample of UNCD that was used in this investigation was not a flat sample; it was convex due to internal stresses caused during the diamond growth process. The AlN was then deposited onto the sample this way. During the photolithography procedure the sample was broken; this caused the AlN layer to break away from the substrate in pieces (flakes). It was at

first assumed that these layers were freestanding AlN, but when held to the light for visual inspection they were not transparent as would be expected. X-ray diffraction was used on one of these flakes to determine why it was not transparent as would be expected and it was found that there was diamond present on the sample. This information was used to also determine that there was good adhesion between the two layers because if there was poor adhesion between the two only AlN would have been present on the XRD analysis. The XRD scan for this sample is shown on the following page, in Figure 40. All the significant peaks are labeled, they are AlN (002), (004) and diamond (111).

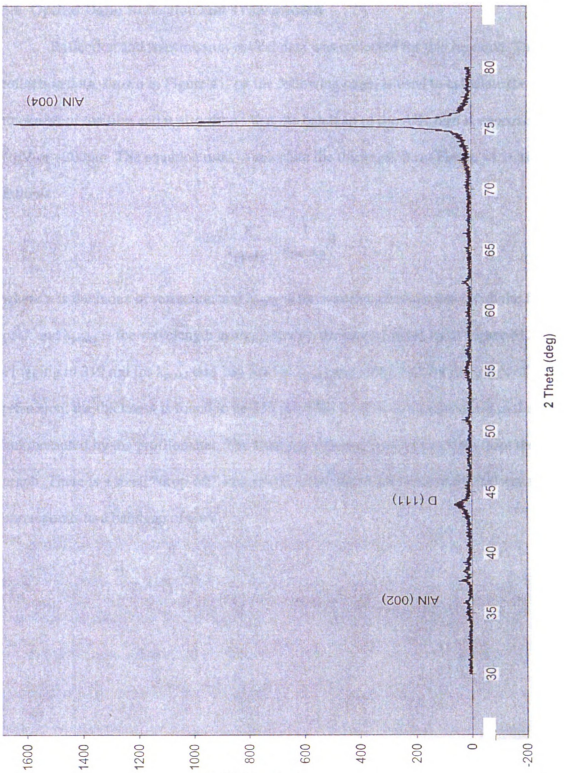

Figure 40 θ-2θ XRD scan for sample CF-022 (XRD scans performed by Rahul Ramamurti)

5.6 Optical Data: Reflection and Transmission

Reflection and transmission optical data was collected for this research. The reflection data, shown in Figure 41, on the following page, is used to calculate the thickness of the film and it also shows that the bandgap of the AlN film is approximately 6 eV or ~200nm. The equation used to calculate the thickness from Figure 41 is as follows

$$t^{-1} = 2n\left(\frac{1}{\lambda_{peak_1}} - \frac{1}{\lambda_{peak_2}}\right) \tag{9}$$

where n is the index of refraction and λ_{peak1} is the wavelength associated with the first peak and λ_{peak2} is the wavelength associated with the second peak, from Figure 41. Plugging in 219 nm for λ_{peak1} and 366 nm for λ_{peak2} and using n=2 for the index of refraction, the thickness is found to be 136 nm. This thickness is pretty close to the 120 nm measured by the profilometer. The bandgap was also found using data from the graph. There is a steep "drop-off" in signal at a lambda of approximately 200 nm and this corresponds to a bandgap of 6 eV.

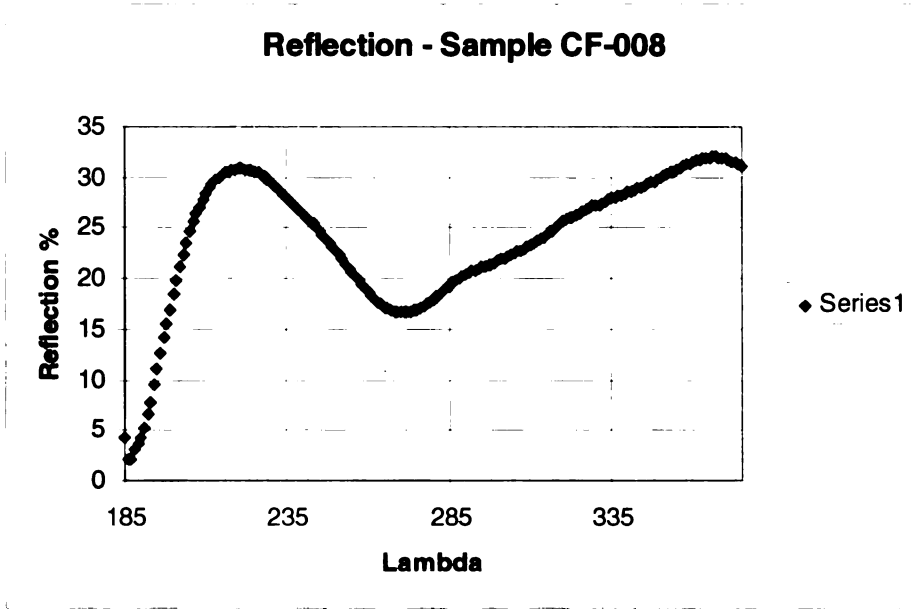

Figure 41 Reflection data collected from sample CF-008

This same methodology was also used to calculate the thickness of sample CF=018. The data for this is shown on the following page in Figure 42. Again, using Equation 9 and plugging in 1615 nm and 2413 nm for λ_{peak1} and λ_{peak2}, respectively and n=2 for the refractive index. The thickness of the sample is then calculated to be 1.22 μm. To confirm this calculation the valleys were also used and the calculation should give the same result. The values of 1393 nm and 1950 nm were used for $\lambda_{valley1}$ and $\lambda_{valley2}$, respectively and n=2 for the refractive index. The thickness was then calculated to be 1.22 μm. This confirms the calculation for the thickness of the AlN film. Although, the peak and the valley calculations of the thickness of the film correspond with each other they do not correspond to the measurements of thickness made by the profilometer, which was 0.8 μm. As mentioned earlier, this could be for a number of reasons. The Dektak needs a sharp step in order to accurately measure the thickness of a film, not a gradual slope (which is what was used in this case because that is all that was available). It could also be due to the fact that the deposited AlN film is not uniform and is thicker in the center

than near the edges of the wafer, which is where the measurements were taken using the profilometer.

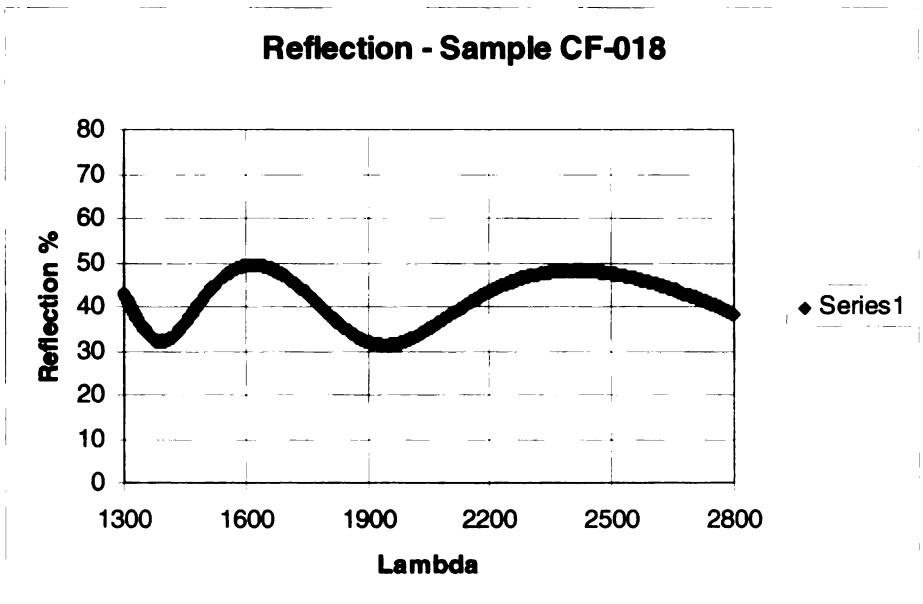

Figure 42 Reflection data for sample CF-018 for a range of 1300 – 2800 nm

Looking at this same data for the range of 185 - 305 nm, as shown in Figure 43 below, it can be seen that the transparency of the film goes to zero at ~230 nm which corresponds to a bandgap of about 5.4 eV.

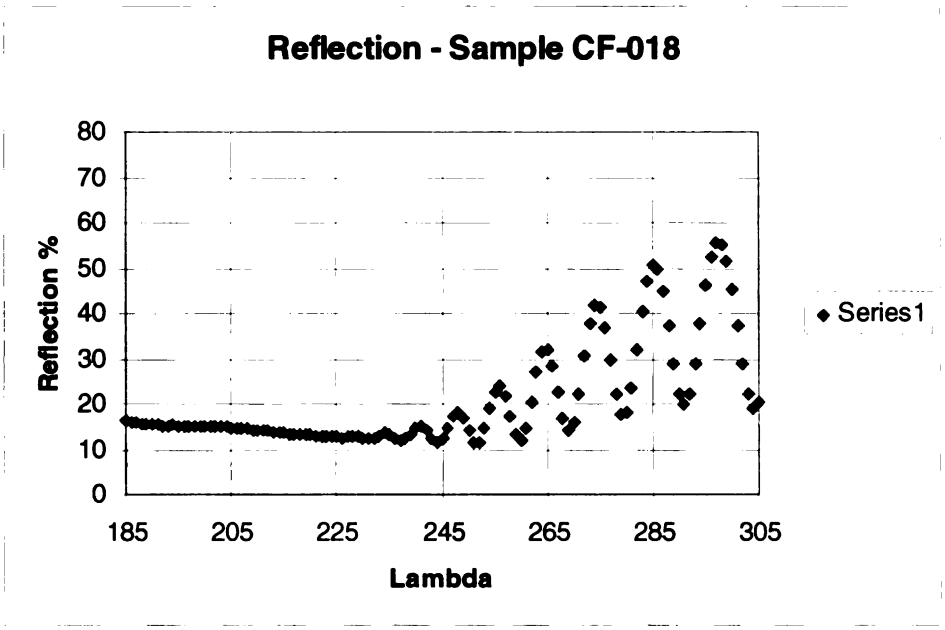

Figure 43 Reflection data for sample CF-018 for a range of 185 – 305 nm

Transmission data was also collected for use in this investigation, as shown in Figure 44 below.

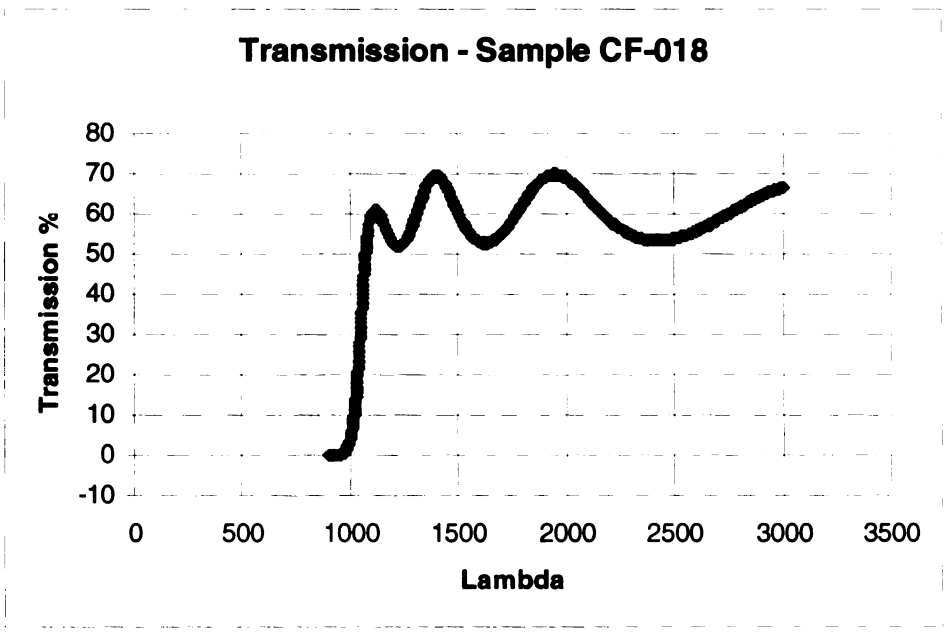

Figure 44 Transmission data for sample CF-018

This set of data shows that the deposited AlN film is transparent causing the constructive and destructive interference. It also shows the onset of absorption by the silicon substrate.

Using Equation 9 again, we can confirm the calculations for the thickness of the film on sample CF-018. For the values of λ_{peak1} = 1396 nm, λ_{peak2} = 1946 nm and n=2 for the refractive index, the thickness of the film is calculated to be 1.23 μm, which is approximately what is found using the reflection data.

5.7 X-Ray Diffraction

The crystal structure of the AlN layer was determined using X-ray diffraction. There were 3 samples that were analyzed using this method. The first sample to be analyzed was CF-022. This sample consisted of four layers, from the bottom up, a silicon substrate, a UNCD layer, an aluminum nitride layer and finally the patterned Al which formed the electrodes. This Al layer, after patterning was only present where there were electrodes, it was not across the entire substrate as the other layers were. The XRD scan for this sample is shown in Figure 40. As discussed earlier this shows that there is AlN film. An interesting point to note is that the (002) is needed for the SAW devices and yet there is only a small signal on the scan. There is however quite a large signal for the (004). X-ray diffraction analysis was also completed for two other samples, CF-021 and CF-008. The θ-2θ XRD scans for these samples are shown below and on the following pages in Figures 45 and 46. As can be seen from both scans there is no significant peak at all other than Si that is picked up by the scan. What has caused this to occur has not yet been assessed, at the time this thesis was written.

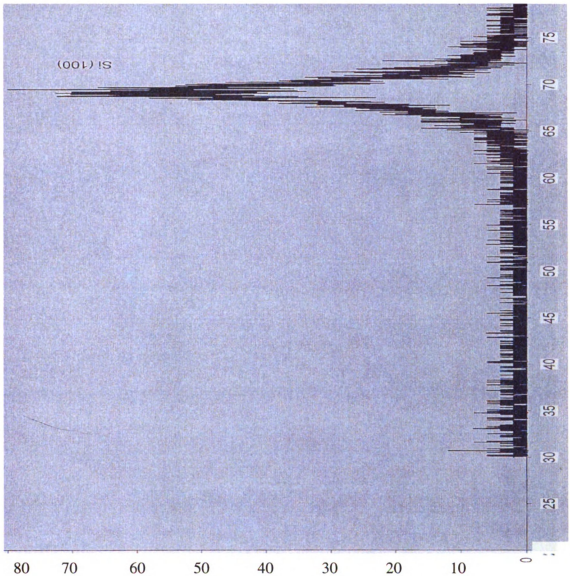

Figure 45 Figure 40 θ-2θ XRD scan for sample CF-008 (XRD scan performed by R. Ramamurti)

Intensity (cps)
2000
1500
1000
500
0
35
40
45
50
55
60
65
70
75
Si (100)

Figure 46 Figure 40 θ-2θ XRD scan for sample CF-021 (XRD scan performed by R. Ramamurti)

5.8 Scanning Electron Microscopy

SEM cross-sectional pictures were taken in order to ascertain what the grain structure of the AlN layer might look like. As shown below in Figure 47 on the following page, a cross-sectional picture was taken with the SEM of sample CF-016. This sample was not coated with a conducting layer of gold (Au) before being placed in the SEM for analysis. Because the AlN and Si layers are not conducting, an image was not obtained, so that the grain structure could be seen under the microscope.

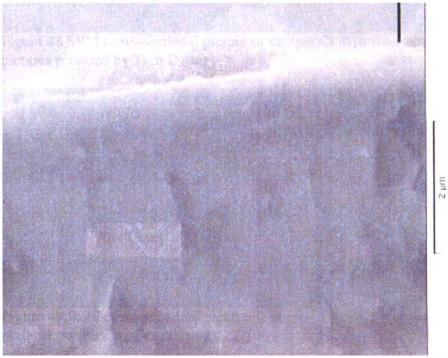

Figure 47 SEM cross-sectional picture of sample CF-016 without Au coating (SEM pictures privided by Tran Dzung)

As can be seen on the following page, in Figures 48, 49, and 50, the grain structure of the AlN layer can be seen. The sample was coated with 20 nm of gold in order to be able to

see the grain structure of AlN layer. It can be seen from these figures that the grain structure is columnar in shape.

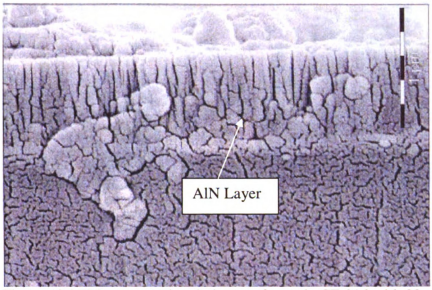

Figure 48 SEM cross-sectional picture of sample CF-016 with 20 nm Au coating (SEM pictures privided by Tran Dzung)

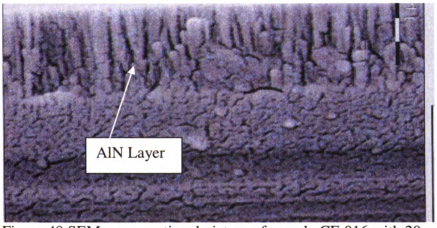

Figure 49 SEM cross-sectional picture of sample CF-016 with 20 nm Au coating (SEM pictures privided by Tran Dzung)

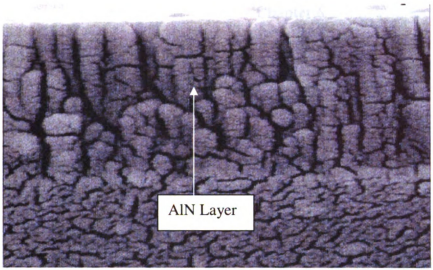

Figure 50 SEM cross-sectional picture of sample CF-016 with 20 nm Au coating (SEM pictures privided by Tran Dzung)

Chapter 6

SAW Device Characterization: Setup and Procedures

6.1 Introduction

This chapter will discuss the characterization techniques, setup and procedures employed in the characterization of the SAW devices. To begin, there will be a description of the network analyzer, Hewlett Packard (HP) 8753 D, and its operating procedures. Next, there is a description of the calibration procedures for the HP 8753D. Then follows, a description of the high frequency probe tips used in order to probe the devices and a description of the probe station and its setup. Finally, there is a discussion of results obtained from a commercial SAW device as well as a SAW device fabricated on quartz using the procedures described in Chapter 3.

6.2 HP 8753D Description and Operating Procedures

In this investigation, a Hewlett Packard (now under the name Agilent Technologies) 8753D network analyzer was used to characterize the SAW devices. The network analyzer allows measurement of the scattering parameters, S_{ij}, of a 'device-under-test (DUT) over a broad frequency range. For example, consider a two port SAW filter with the input terminal connected to port 1 of the spectrum analyzer and the output terminal connected to port 2. The S_{ij} are defined as

$$S_{ij} = \frac{v_i^-}{v_j^+} \tag{10}$$

where v_j^+ is the amplitude of the voltage wave incident on the DUT from port j and v_i^- is the amplitude of the voltage wave reflected from the DUT to port i. Thus, as described by Pozar, "S_{ij} is found by driving port j with an incident wave of magnitude v_j^+ and measuring the reflected wave amplitude v_i^- coming out of port i" [43]. This is accomplished by the 8753D. For a SAW filter, as illustrated, for example, in Figure 3 of Chapter 2 and Figure 9 of Chapter 3, one wishes to have a high transmission from port 1 to port 2, or in other words, a large value of S_{12}, at resonant frequency. At non-resonant frequencies, S_{12} should be low. A picture of the network analyzer is shown below, in Figure 51.

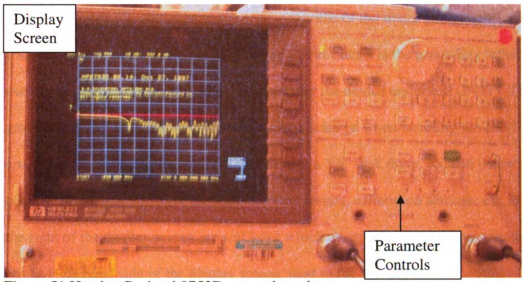

Figure 51 Hewlett Packard 8753D network analyzer

This will not be an in-depth description of the network analyzer, but all the parameters vital to conducting the necessary measurements on the SAW devices will be discussed. On the left hand side of the HP 8753D is the display screen and on the right hand side of the machine are the parameter control buttons, as shown above in Figure 51.

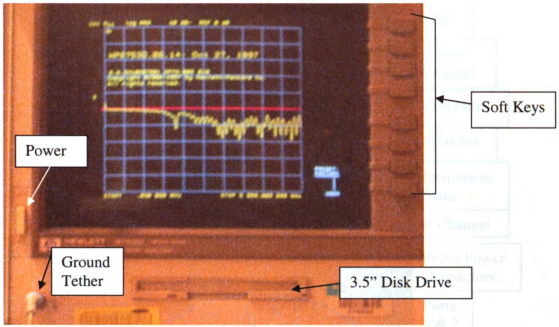

Figure 52 HP 8753D display and other components

Shown in Figure 52, on the previous page, are some of the major components associated with the display screen. The plug below the power button is the grounding tether for the user to wear when connecting and disconnecting the device under test (DUT). This tether grounds the user to avoid an accidental static discharge when handling the DUT which could potentially harm the device. There is also a 3.5" disk drive, located below the display, so the user can save the measurement results, calibration settings, etc. Directly to the right of the display screen are soft keys which allow the user to access menus shown on the right hand side of the display screen, next to the soft keys.

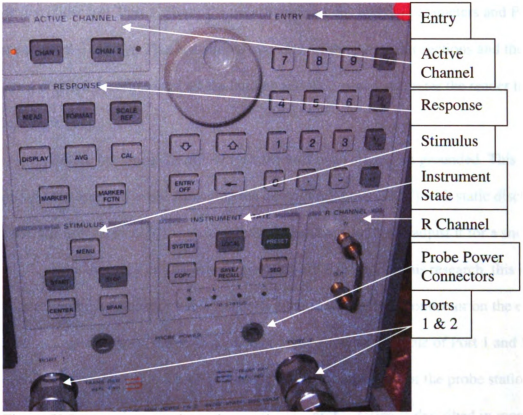

Figure 53 Parameter control panel

In Figure 53, shown above, the keys to control the measurement parameters are organized in sections which are labeled both on the photograph and with side captions. The two Active Channel buttons are independent display channels and these keys allow you to choose the active channel. The functions then chosen apply to the channel that is active at the time [44]. Just below these buttons are the Response keys. The Response keys allow the user to control the measurement and display parameters. The Stimulus buttons control parameters such as frequency, power, etc. The Entry block of keys is for entering numerical data and controlling the markers. In the box marked Instrument State are the keys which control channel-independent system functions, such as save/recall, tuned receiver mode and test sequence function. Finally, at the bottom of the figure are Ports 1 and 2 which give an output signal from the source and receive an input signal from the

device under test. Port 1 allows the user to measure S_{11} and S_{12} parameters and Port 2 measures S_{22} and S_{21}. This is a simple overview of the parameter sections and their uses. For a detailed description of all the buttons and their uses I will refer the reader to reference [44].

Before operating the HP 8753D, the user must always be grounded. This will ground the user and avoid damaging the device under test (DUT) with static discharge. First, the user must slide the ground tether around the wrist and adjust it for a snug fit.

Now the DUT can be connected to the HP 8753D. For this research, this includes connecting high frequency cables to Ports 1 and 2 with a male connector on the end. For non-packaged devices, the male connector at the end of each cable of Port 1 and Port 2 needs to be connected to a high frequency probe on either side of the probe station as shown in Figure 57, on the following page. The probe station is described in more detail in section 6.4. The Ports must be connected to ONLY those connections pointed to in Figure57, because these are the only connections for the high frequency probes on the probe station. For procedural purposes, Port 1 will always be connected to the connector shown on the left and Port 2 will always be connected to the connector pointed to on the right (which is beneath a metal shield, but the connector is the same as that shown to the left in the figure).

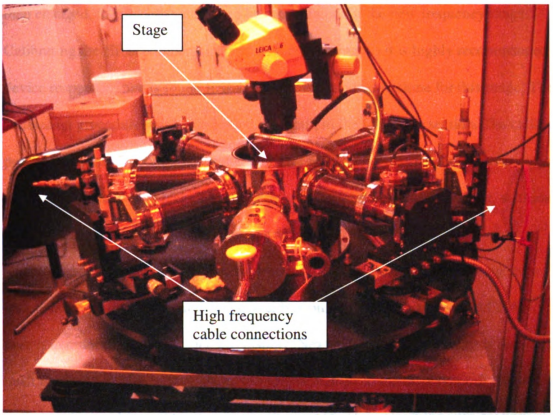

Figure 54 Probe station connected to the HP 8753D in order to characterize the DUT

Now that the HP 8753D is connected to the probe station, the DUT is placed on a stage inside the probe station. The stage is located inside the cavity, as shown in Figure 54. The wafer containing the SAW devices is placed on the stage and the DUT (the SAW device probed by the user) is connected to the probes. The setup/configuration of the probes and the probing of the DUT will be explained, in detail, in section 6.3.

In order to account for mismatch in impedance and channel cross-talk, the HP 8753D needs to be calibrated, before measurements are taken. However, if there is any uncertainty in what range the frequency response for the device lies, I would suggest doing preliminary measurements to find the device response, then calibrate the machine for this range and then take measurements. This would be beneficial and time saving because once the machine is calibrated for a specific frequency range and that range is

then changed, the machine must then be recalibrated for the new frequency range. Calibrating the HP is cumbersome and time consuming, so it is highly recommended that device response range is found first and then calibrate the machine for this range. The calibration procedure will be discussed, in detail, in the following section. The calibration procedure involves setting the frequency range for which the s-parameter measurements will be taken and it also includes setting the number of points and averaging, so these steps do not need to be included in this section.

In order to measure the s-parameters of the SAW device the following steps should be followed. In the Active Channel box on the HP 8753D, push the CHAN 1 button in order to select channel 1 to display. Next, under the Response area on the HP, push the SCALE REF button. Using the soft keys, next to the display, push the soft key with AUTO SCALE next to it on the display screen. This selects the auto-scaling function for the display. Next, under the Response area, push the button labeled FORMAT. Using the soft keys, push the soft key with LOG MAG next to it on the display screen; this displays the magnitude of the DUT on a logarithmic scale. Now press the button labeled MEAS, in the Response box, on the HP 8753D. Finally, using the soft keys choose which s-parameter to measure. The S11 parameter is the reflection coefficient of the forward traveling wave, S12 is the transmission coefficient for the forward traveling wave, S21 is the transmission coefficient for the reverse traveling wave and S22 is the reflection coefficient for the reverse traveling wave.

6.3 HP 8753D Calibration Procedures

In order to optimize the measurements of the S-parameters of the SAW devices, the HP 8753D needs to be calibrated by doing a TRL (Through, Reflect Line) calibration.

For packaged devices to which simple cable connections can be made, one uses the HP 'calibration kit standard'. However, for devices tested with the probe station, one must modify the calibration kit standard to a user defined standard as the first step of the process. The second step is to perform the TRL calibration using an impedance standard for the 3 input high frequency probes. The steps for both of these procedures can also be found in reference [44], which is the Hewlett Packard 8753D User's Guide.

The substrate used as an impedance standard was Model 101-190 from Cascade Microtech, Incorporated [45]. This is a 0.8 x 0.6 x 0.025 inch aluminum oxide substrate, on which are repeated arrays of metallization patterns corresponding to 50 ohm loads, 'shorts' and 'thru' lines. When a probe is placed on a 50 ohm load metal pattern, a precise 50 ohm load is presented between signal and ground for that probe. When a probe is placed on a short, the signal is shorted to ground. An open circuit is synthesized by raising the probes in the air at least 250 μm above the surface. When the probe is placed on a thru line, it may be directly connected to an opposing second probe also placed on the same through line. In this case, two probes are connected ground-to-ground and signal-to-signal with a 1 ps delay between them. Also, on the impedance standard are thru lines with longer delays, up to 40 ps for a length of 5.25 mm. The three different types of calibration pads are shown generically in Figure 55, on the following page. There are 40 of each type on the chip, as well as several thru lines with longer delays.

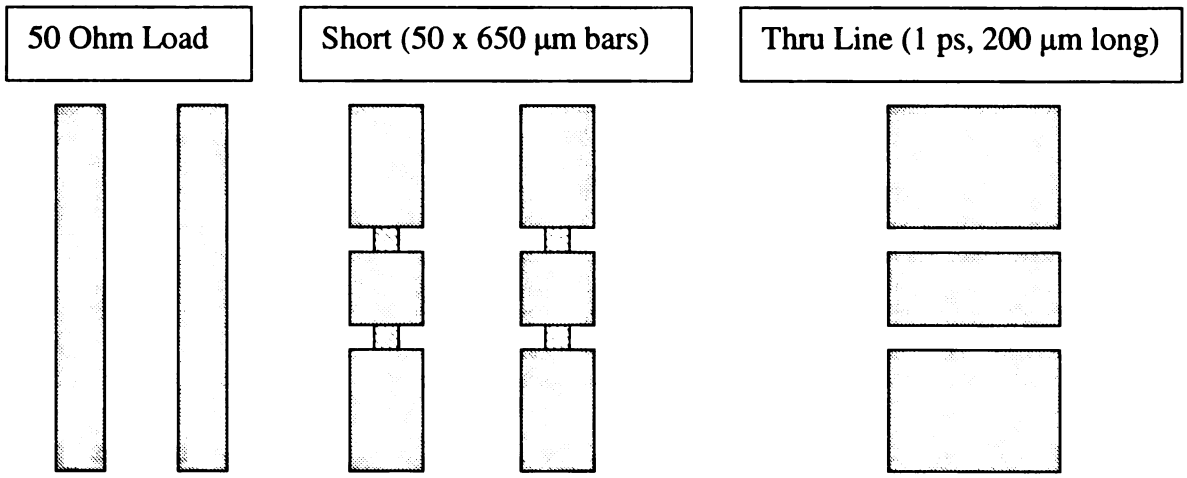

Figure 55 Metalized patterns on the calibration standard

These are the steps that need to be followed in order to switch from 'calibration kit standard' to 'user defined standard'. Push the button labeled CAL, located in the Response area of the HP 8753D. Now using the soft keys, select CAL KIT, then MODIFY and then DEFINE STANDARD. Next, to select a short, press 1 and then the x1 button (the reflect standard is a short for our purposes). Next, press SHORT, then SPECIFY OFFSET and OFFSET DELAY. To set this delay to 0 seconds, press 0, x1, STD OFFSET DONE and then STD DONE (DEFINED). Next, define the thru/line standard. To do this, press DEFINE STANDARD, 4 and x1. Then press DELAY/THRU, SPECIFY OFFSET, OFFSET DELAY, 1, and x1. The number one is selected here because the delay/thru line on the standard has a 1 picosecond delay and not 0 as ideally noted in the HP User's Guide. Now press STD OFFSET DONE and then STD DONE (DEFINDED). Next, to define the line/match standard press DEFINE STANDARD, 6, x1. To set the delay for the line standard push DELAY/THRU, SPECIFY OFFSET, OFFSET DELAY, .04 and G/n. For the standard used this sets the delay at 40 picoseconds as specified by the standard verification line. Now press STD OFFSET DONE.

The standards are now defined and the labels for these standards can be changed for clarity. Press LABEL STD and using the knob in the next to the keypad modify the name to LINE. When the new name appears press, DONE and STD DONE (DEFINED).

Now we need to assign the standards to TRL classes. In order to do this press, SPECIFY CLASS, MORE, MORE, TRL REFLECT. Because the number 1 was selected for the Reflect standard earlier press 1 and then x1. The number 6 was used for the line/match standard press, TRL LINE OR MATCH, 6 and x1. The number 4 was used for the thru/line standard press, TRL THRU, 4 and x1. The assignment of TRL classes is now finished, press SPECIFY CLASS DONE.

Next we need to label the classes we have just assigned. Press LABEL CLASS, MORE and MORE. Change the label of the TRL REFLECT class to TRL SHORT, then change the label of TRL LINE OR MATCH class to TRL LINE and lastly change the label of the TRL THRU class to TRL THRU. Now press LABEL CLASS DONE.

Finally, we need to label the calibration kit. Press LABEL KIT and name the kit using a maximum of 8 characters and then press DONE. In order to save the kit in non-volatile memory press KIT DONE (MODIFIED) then SAVE USER KIT. A user defined kit has now been defined and can now be used to calibrate the HP 8753D.

Before beginning the calibration, there are some parameters that need to be set first. In the box labeled Response on the HP 8753D, push the button labeled AVG. Using the soft keys push the one labeled AVERAGING and turn the averaging ON. Now push the button labeled MENU in the Stimulus area on the HP 8753D. Using the soft keys, push the one labeled NUMBER of POINTS and select the number of sampling points to be taken, 201 points were used in this research. This is enough points to get an accurate

measurement and not too many so that the measurement takes too much time. Finally, the frequency range needs to be set. Push the button labeled START in the Stimulus box on the HP and type in the starting frequency, using the number pad or use the knob to dial in the correct starting frequency and push the appropriate label, e.g. k/m for kHz or M/u for MHz. Push the STOP button in the Stimulus box on the HP and type in the stopping frequency and then push the appropriate label button as explained previously.

The HP is now ready to be calibrated to the probe station. There must be a TRL calibration kit defined and saved in the USER KIT. To begin the calibration, press the button labeled CAL in the Response section of the HP 8753D. Using the soft keys, push CAL KIT, SELECT CAL KIT, USER KIT and RETURN. Now push, CALIBRATE MENU and TRL/LRM 2-PORT. To measure the TRL THRU, place the probes on either end of the, 1 ps, thru line on the calibration standard and press THRU TRLTHRU (or whatever you labeled this action in the user kit defined previously). When the measurement is completed the name will be underlined. To measure the TRL SHORT, place each probe on a short bar located on the calibration standard. To measure the reflection from port 1, press S11 REFL: TRLSHORT and to measure port 2, press S22 REFL: TRLSHORT. Now place the probes at either end of the longest thru verification line, the same one you defined with a delay of 40 picoseconds when defining the calibration user kit. Press LINE/MATCH and DO BOTH FWD + REV. For this research the Isolation calibration did not need to be performed and for this simply push OMIT ISOLATION and then DONE TRL/LRM. The HP then calculates the calibration coefficients, when it has finished with the calculations the DUT may be attached and the s-parameters may be measured. Again, as mentioned, before the same frequency range

used for calibration must be used when measuring the s-parameters otherwise the calibration is null and void and the HP must be recalibrated. An error message will appear on the display stating that calibration coefficients will be turned off (not used) if the frequency range is changed and a prompt will ask to confirm that the change in frequency will turn off the calibration coefficients.

6.4 Probes/Probe Station Description

Due to the small size of the SAW devices and the frequency range in which they are designed to operate, high frequency probes with micrometer size contacts are required to probe and characterize the SAW devices. The use of these probes also requires the use of a probe station. The probe station allows for the substrate to be held motionless and to be unaffected by vibration while it is being probed.

The high frequency probes are co-planar coaxial probes. The frequency range for the probes used in this research is DC to 40 GHz, with an insertion loss of less than .8 dB. The structure for these probes is a ground-signal-ground (GSG) structure; this means that there are three co-planar contacts. The outside contacts are the ground contacts and the center contact carries the signal. In Figure 56, on the following page, is a picture of the high frequency probe used in this research.

Figure 56 High frequency probe

The probes are connected to the probe station, as shown below, in Figure 57.

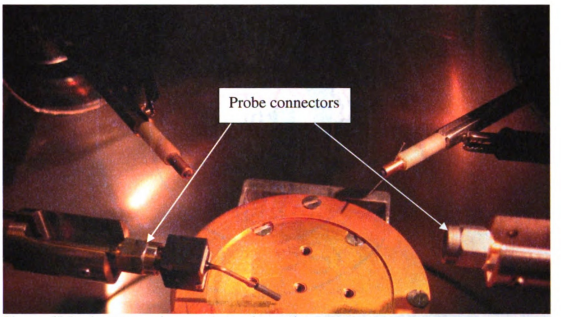

Figure 57 Probe connections to the probe station

Extreme care and caution must be taken when handling the probes. Avoid getting anything near the probe tips. This includes hands and fingers, as they are fragile and are easily broken. To attach the probes, screw them in to the connectors, as labeled in the figure above. It is easiest to attach the probes prior to connecting the cables from the HP 8753D. The probe connectors can be rotated with a wrench to connect the probes, as

labeled in Figure 57. If the probes are attached in this way, it avoids the issue of having to rotate the actual probe to screw them in place, which increases the chances damaging the probe tips. Always be sure to remove the probes from the probe station and put them away upon finishing taking measurements.

The probe station used in this research, was shown earlier in this chapter and is shown below in Figure 58 with different attributes labeled. A nitrogen tank is connected to the probe station which supplies a steady flow of gas to the legs of the table on which the probe station sits. This flow of gas allows the table to "float" on a layer of nitrogen, isolating the table from the ground. Isolating the table (i.e. the probe station) from the ground keeps vibrations from effecting the measurements.

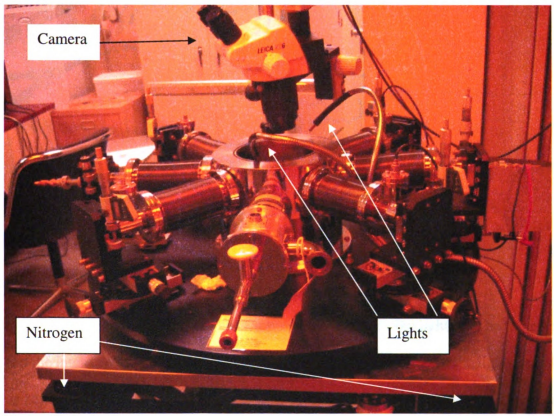

Figure 58 Probe Station

The camera is connected to a television monitor. Turn the monitor on and this allows the user to see the substrate without leaning over probe station, which would risk disturbing or perhaps damaging the substrate and/or the devices if the probe station is accidentally bumped. The camera also allows the user to zoom in/out in order to see one device, one section of a device, etc. For this research, it was used to see the input/output contact pads on the device to ensure that all three points of the probes were making contact with the pads. If the probe is not properly making contact then the s-parameters would not be correct.

The lights can be turned on via a power box near the probe station, shown below in Figure 59.

Figure 59 Power box for the probe station lights

By turning the knob on the right-hand side of the power box the lights can be turned on and the intensity of the lights can be adjusted as well. The position of the lights can also be adjusted so the light can be focused anywhere the user chooses. There tends to be a glare from the light, making it difficult to see, if it is focused directly on the DUT; so

adjusting the position of the lights is important to avoid this glare and have a clear view of the DUT.

The device under test is placed on the stage located inside the probe station as can be seen in Figure 60, below.

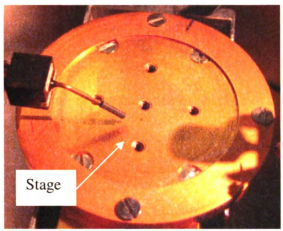

Figure 60 Stage located in the probe station

Before placing the substrate on the stage be sure that the probes (if already attached to the probe station) are moved as far back, away from and above, the stage as they can be moved; this is done in order to minimize the risk of damaging the probe tips.

6.5 Measurements/Results

S-parameter measurements were taken of several devices. To begin, measurements were taken of two commercial devices; both were the same type of device (a SAW filter), made by the same manufacturer, but one device measurement was taken with the packaging in tact and the other device was measured with the top portion of the packaging removed. The samples were mounted, as shown on the following page in Figure 61, so the devices could be connected to the HP 8753D network analyzer. The samples were mounted by another graduate student working with Dr. Ed Rothwell.

Figure 61 Mounted commercial SAW device

The characterization results of the commercial devices varied drastically, depending on the presence or absence of chip packaging. For the device with the top part of the packaging removed the s-parameter measurement of the transmission parameter, S_{21}, resulted in a line beginning at -85 dB and decreasing to approximately -95 dB, behaving pretty much like an open circuit, as shown below in Figure 62.

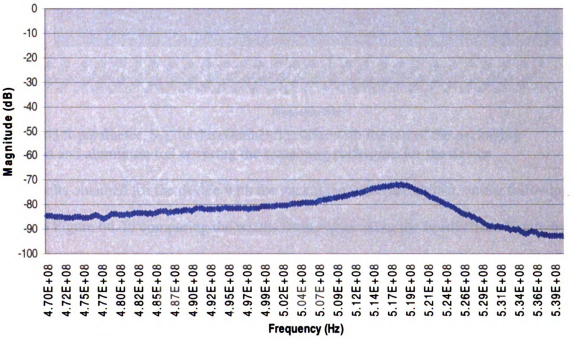

Figure 62 S-parameter, S_{21}, of the commercial filter with the top of the packaging removed

After placing a small piece of aluminum foil over the top of the remaining packaging, results were obtained which were similar to the results of the device with the packaging

still intact. The s-parameter result for the device with the cap off and the aluminum foil covering the remaining packaging are shown on the following page, in Figure 63.

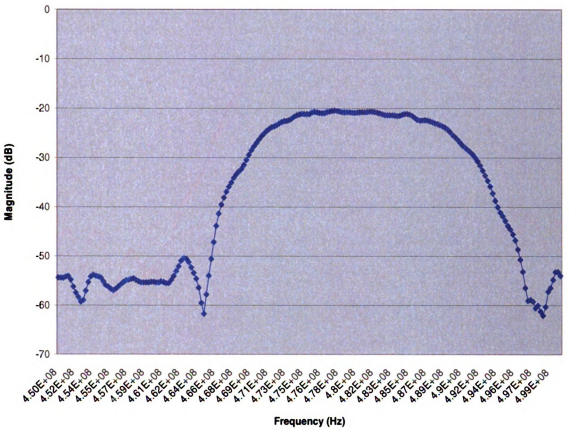

Figure 63 S-parameter, S_{12}, of the commercial filter with the top of the packaging removed and aluminum foil covering the remaining packaging for the device

The results obtained for the device with the packaging intact are shown, on the following page, in Figure 64. In comparing the results from Figure 63 to the results from Figure 64, they are similar. Figure 63 shows the transmission s-parameter (S12) results for the commercial SAW filter. The insertion loss is approximately -20 dB and the center frequency is approximately 480 MHz; these parameters match with those given in the device data sheet, reference [46]. Figure 64, for the commercial device that was left intact and measured, shows similar results. The insertion loss is approximately -20 dB and the

center frequency is approximately at 480 MHz, which again matches the manufacturer's data sheet specifications.

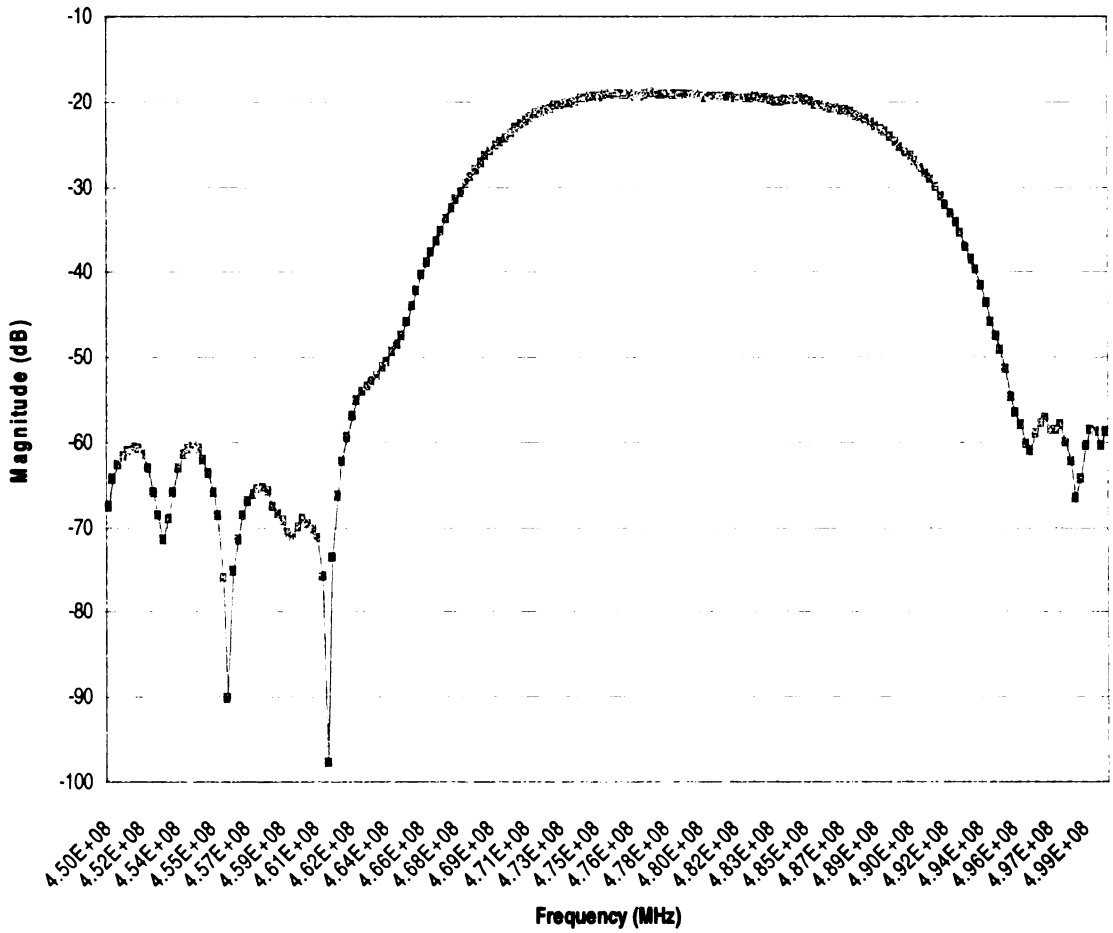

Figure 64 S-parameter, S_{21}, of the commercial filter with the packaging in tact

The S_{21} parameter was investigated for a SAW structure formed by aluminum electrodes deposited on an ST-cut quartz substrate during the course of this research. The aluminum was deposited as described in chapter 3 and patterned using the electrode mask pattern described in chapter 4. The preliminary results obtained for the s-parameter measurement of the experimental SAW device (SAW filter) is shown on the following page in Figure 65.

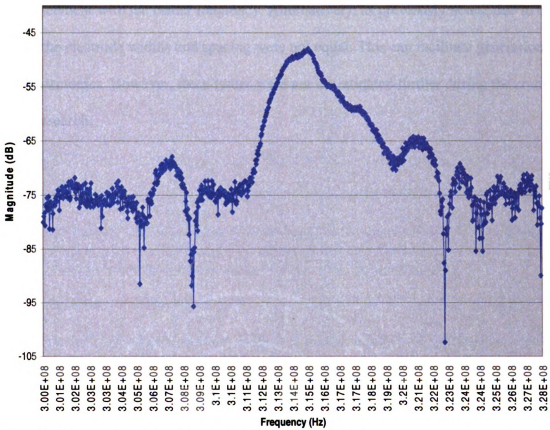

Figure 65 S-parameter, S_{21}, of the experimental SAW filter

These results are for an uncalibrated frequency scan using the probe station and the network analyzer as explained in the previous section of this chapter. A band-pass frequency centered at approximately 315 MHz with a height of about 18 dB is illustrated. The band-pass is not as well shaped as the packaged commercial device. This may be partly due to the fact that the probed device was still on the quartz wafer, unpackaged and also because the analyzer had not been calibrated.

It was realized after-the-fact that the center frequency is higher than would be expected for the ST-cut quartz surface wave, which is 3080 m/s. Using Equation 5 and a wavelength of 16 μm, the expected resonance would be at about 190 MHz. One possible explanation for this is that the IDT structures can also excite bulk acoustic waves to various extents. The bulk wave velocity would be approximately 5000 m/s which would

be in agreement with the center frequency. Alternatively, as previously noted, due to over etching the electrode widths and spacing were not equal. This can facilitate generation of higher harmonics. However, these issues were not investigated further during the course of this research.

Chapter 7

Conclusions

7.1 Introduction

This chapter will discuss conclusions based on the results found in the previous chapters. It will also cover future work to be done with this project.

7.2 Conclusions

For the fabrication of the electrodes, it is paramount that the spacing and width of the electrodes are calculated and fabricated properly for the desired operating frequency of the device. Using Equation 5 one can calculate the wavelength. Then using the calculated wavelength and Equation 6 the necessary IDT width (and hence the spacing between the fingers) can be calculated. For this investigation the wavelength was calculated to be 16 μm, using the desired operating frequency of 500 MHz. Using the calculated wavelength, the necessary IDT width, for achieving the desired center frequency, was found to be 4 μm. The aluminum layer must be uniform and one must take care not to over etch when patterning the electrodes, otherwise they will be too thin and will not work properly. The aluminum layer was successfully patterned to form the IDTs for the SAW devices. For each IDT 20 pairs of electrodes were formed for some of the SAW devices. The actual width of the electrodes and the spacing between them were 2.3 μm and 5.7 μm, respectively. In order to get a functioning SAW device, the proper equipment needs to be used for fabricating these devices. There needs to be a proper

cleanroom environment in order to fabricate the electrodes. Due to their small size, 4 μm, it is easy for particles to wreak havoc on the electrode fabrication process (the photolithography steps).

There were two different SAW devices that were fabricated, a filter and an oscillator. There were also different variations of each of these devices. Some of the variations include inductors at one end of each IDT, different size electrodes (larger or smaller width) and hence spacing between the fingers as well and different numbers of electrodes on some devices.

Using a reactive dc pulsed sputter process for the deposition of aluminum nitride (AlN), a range of parameters were investigated. Some of these parameters include frequency, reverse time, power, deposition pressure, distance to target and substrate temperature. The recommended parameter settings for deposition frequency set to 50 kHz, the reverse time set between 3 – 5 μs, power set between 375 and 450 W, set the deposition pressure to 3 mTorr, the distance to the target should be 7.5 cm, and the substrate temperature used was 350° C . It is vital to have the right substrate temperature in order to get the (002) facing for the AlN layer; this allows for the desired piezoelectric effect in the AlN. At the time of writing this thesis getting the (002) facing for the AlN has been illusive. The full set of parameter settings are listed in Tables 8 – 10 in chapter 4. The reason for the range on the reverse time and the power is due to chamber conditions. For each run the chamber conditions are different and as the run is in progress the chamber conditions are constantly changing. The power and the reverse time are set based on these conditions. With these parameter settings the AlN layer had a thickness

that ranged from 187 nm – 1500 nm, for different deposition times ranging from 35 – 163 minutes. The Young's Modulus for some of these samples ranged from 280 – 353 GPa.

The AlN layer also does not need to be too thick but getting the appropriate thickness is important. The normalized thickness needs to be .2 because this corresponds to the maximum electromechanical coupling coefficient. In this investigation the thickness of the AlN layer needs to be 500 nm thick. To get good deposition rates an arc-less process can not be used, it would take hours in order to get the appropriate thickness of AlN. The deposition rates for an arcless process range from 40 – 70 nm/hr as compared to a range of 150 – 550 nm/hr for a process that produced some arcing.

The resulting layer of AlN is transparent with an optical gap of approximately 6 eV or 200 nm. These results are consistent with literature values for AlN. Preliminary XRD (x-ray diffraction) results show a small peak signal at 36° for AlN (002) and a significant AlN (004) peak at ~76°. This scan was performed on an AlN layer deposited on UNCD. Results for samples on silicon were inconclusive. The scans show no peaks for AlN at all, not even for Al or N. But based on other data and a simple visual inspection it can be seen that there is a layer of AlN on the substrate. Further XRD scans would be beneficial. The surface roughness of the AlN layer, as measured on sample CF-018 (on a Si substrate), was low with an Ra of 0.78 nm and an Rz value of 28.77 nm. This means the deposited layers were smooth after deposition. The deposited layer also had good adhesion to the substrate and has a columnar grain growth structure as would be expected. The deposited layer is uniform if the substrate is rotated during deposition but this cuts the deposition time as well. The appropriate heating and power need to be used

in order to get the (002) plane to grow, but this has been proven to be difficult on the PVD 75 system.

The diamond layer needs to be at least 2 – 3 λ thick so that the velocity of the SAW is not adversely affected by the substrate layer, which has a much lower phase velocity than the diamond. In our case, it needed to be 10 μm thick. Such a wafer was provided for this research with UNCD deposited by Tran Dzung and was polished by Martin Kutchler.

An AlN layer was successfully deposited on UNCD, specifically AlN/UNCD/Si were the order of the layers. Al was also deposited on the AlN layer in order to form the IDTs for the SAW devices. However it was not possible to etch and pattern the aluminum because the wafer was damaged during the lithography step of processing. Due to internal stresses in the diamond layer the sample had significant bowing effects. The lithography step includes a contact mask, where the sample must be flush against the mask for the photoresist to be fully exposed. When the wafer was put in contact with the mask it broke into pieces too small to work with and the layers of AlN and diamond flaked off the Si substrate. For future work the internal stress/bowing issue needs to be addressed and/or working with smaller samples. However, SAW devices were successfully fabricated on a quartz – ST substrate. A signal was obtained using an HP 8753D network analyzer as verification that the devices would work as designed.

The diamond layer needs to be at least 2 – 3 λ thick so that the velocity of the SAW is not adversely affected by the substrate layer, which has a much lower phase velocity than the diamond. In our case, it needed to be 10 μm thick. Such a wafer was

provided for this research with UNCD deposited by Tran Dzung and was polished by Martin Kutchler.

APPENDIX

List of Samples

Table 15 Deposition parameters for AlN samples

Sample #	Reverse Time (us)	Deposition Pressure (mTorr)	Frequency (kHz)	Power (W)	Substrate Temperature (° C)	Distance to Target (cm)	Rotation
CF-001	10	7.5	50	187	0	15	Yes
CF-002	10	7.5	50	200	0	15	Yes
CF-003	10	12	50	186	0	15	Yes
CF-004	10	7.5	50	201	0	15	Yes
CF-005	10	12	50	203	0	15	Yes
CF-006	10	7.5	50	221	0	15	Yes
CF-007	10	7.5	50	x	0	15	Yes
CF-008	10	7.5	50	200	0	15	Yes
CF-009	10	7.5	50	205	0	7.5	No
CF-010	10	7.5	50	205	0	7.5	No
CF-011	10	7.5	50	225	0	7.5	No
CF-016	2 - 5	3 - 10	30 - 70	300 - 500	0	7.5	No
CF-017	1 - 10	3	20 - 100	223 - 500	0	7.5	No
CF-018	4	3	50	420	0	7.5	No
CF-019	3	3	50	434 - 450	0	7.5	No
CF-020	5	3	50	364 - 420	350	7.5	No
CF-021	5	3	50	361 - 391	350	7.5	No
CF-022	5	3	50	367 - 375	350	7.5	No

Samples CF–012 to CF-015 were not AlN samples and were unrelated to this thesis research and therefore are not included in Tables 15 and 16.

Table 16 Layer characteristics for AlN samples

Sample #	Deposition Rate (nm/hr)	Deposition Time (min)	Layer Thickness (nm)	Young's Modulous* (Gpa)	Surface Roughness (nm)	Color	Uniform
CF-001	70.2	65	76	x	Ra = 1.8	Clear	Yes
CF-002	57	60	57	x	Ra = 2.5	Clear	Yes
CF-003	62	60	62	x	x	Clear	Yes
CF-004	40	60	40	x	x	Clear	Yes
CF-005	x	60	x	x	x	Clear	Yes
CF-006	x	60	x	x	x	Clear	Yes
CF-007	x	60	x	x	x	Clear	Yes
CF-008	60	120	120	150	x	Royal Blue	Yes
CF-009	150	120	300	x	x	Blue, Purple, Yellow	No
CF-010	x	160	x	x	x	x	No
CF-011	x	600	x	x	x	x	No
CF-016	462.2	64	493	280	x	Purple, Green	No
CF-017	552.1	163	1500	330	Ra = 1.57, Rz = 45.17	Purple, Yellow, Green	No
CF-018	400	120	800	353	Ra = .78, Rz = 28.77	Purple, Yellow, Green	No
CF-019	320.6	35	187	x	Ra = 2.07, Rz = 7.28	Pink, Green	No
CF-020	255.8	120	512	x	Ra = 7.8, Rz = 47.71	Blue, Pink, Green, Purple, Yellow	No
CF-021	395.5	130	857	x	x	Blue, Pink, Green, Purple, Yellow	No
CF-022	x	104	x	x	x	Blue, Pink, Green, Purple, Yellow	No

*Young's Modulous measurements provided by M. K. Yaran.

REFERENCES

References

1. U. Wolff, F. L. Dickert, G. K. Fischerauer, W. Greibl, C. C. W. Ruppel, "SAW Sensors for Harsh Environments," IEEE Sensors Journal, Vol. 1, No. 1, pp. 4-13, June 2001

2. R. Weigel, D. P. Morgan, J. M. Owens, A. Ballato, K. M. Lakin, K. Hashimoto, C. C. W. Ruppel, "Microwave Acoustic Materials, Devices and Applications," IEEE Transactions on Microwave Theory and Techniques, Vol. 50, No. 3, pp. 738-749, Mar. 2002

3. R. A. McGill, R. Chung, D. B. Chrisey, P. C Dorsey, P. Mathews, A. Pique, T. E. Misna, J. L. Stepnowski, " Performance Optimization of Surface Acoustic Wave Chemical Sensors," IEEE Transactions on Ultrasonics, Ferroelectrics and Frequency Control, Vol. 45, No. 5, pp.1370-1380, Sept. 1998

4. L. M. Reindl, A. Pohl, G. Scholl, R. Weigel, "SAW-Based Radio Sensor Systems," IEEE Sensors Journal, Vol. 1, No. 1, pp. 69-78, June 2001

5. J. T. Glass, B. A. Fox, D. L. Dreifus, B. R. Stoner, "Diamond for Electronics: Future Prospects of Diamond SAW Devices," MRS Bulletin, pp. 49-55, Sept. 1998

6. H. Meier, T. Baier, G. Riha, "Miniaturization and Advanced Functionalities of SAW Devices," IEEE Transactions on Microwave Theory and Techniques, Vol. 49, No. 4, pp. 743-748, Apr. 2001

7. H. Nakahata, S. Fujii, K. Higaki, A. Hachigo, H. Kitabayashi, S. Shikata, N. Fujimori, "Diamond-Based Surface Acoustic Wave Devices," IoP Electronic Journals, Semiconductor Science and Technology, Vol. 18, No. 3, S96-S104, Mar. 2003

8. S. Shikata, H. Nakahata, A. Hachigo, N. Fujimori, "High Frequency Bandpass Filter Using Polycrystalline Diamond," Diamond and Related Materials, 2, pp. 1197-1202, 1993

9. S. Shikata, H. Nakahata, A. Hachigo, "New Material Systems for Diamond Surface Acoustic Wave Devices," New Diamond and Frontier Carbon Technology, Vol. 9, No. 1, pp. 75-92, 1999

10. K. Higaki, H. Nakahata, H. Kitabayashi, S. Fujii, K. Tanabe, Y. Seki, S. Shikata, "High Power Durability of Diamond Surface Acoustic Wave Filter", IEEE Transactions on Ultrasonics, Ferroelectrics and Frequency Control, Vol. 44, No. 6, pp.1395-1400, Nov. 1997

11. M. Ishihara, T. Nakamura, F. Kokai, Y. Koga, "Preparation of Lithium Niobate Thin Films on Diamond-Coated Silicon Substrate for Surface Acoustic Devices," Diamond and Related Materials, 12, pp. 1809-1813, 2003

12. V. Mortet, M. Nesladek, J. D'Haen, G. Vanhoyland, O. Elmazria, M. B. Assouar, P. Alnot, M. D'Olieslaeger, "Deposition of Aluminum Nitride Film By Magnetron Sputtering for Diamond-Based Surface Acoustic Wave Applications," Physica Status Solidi (a), Vol. 193, No. 3, pp. 482-488, 2002

13. P. R. Chalker, T. B. Joyce, C. Johnston, J. A. A. Crossley, J. Huddlestone, M. D. Whitfield, R. B. Jackman, "Fabrication of Aluminum Nitride/Diamond and Gallium Nitride/Diamond SAW Devices," Diamond and Related Materials, 8, pp. 309-313, 1999

14. H. Nakahata, A. Hachigo, K. Higaki, S. Fujii, S. Shikata, N. Fujimori, "Theoretical Study on SAW Characteristics of Layered Structures Including a Diamond Layer," IEEE Transactions on Ultrasonics, Ferroelectrics and Frequency Control, Vol. 42, No. 2, pp. 362-375, May 1995

15. D. M. Gruen, A. R. Krauss, US Patent Specification No. 5.772.760, 1998

16. D. M. Gruen, Annual Review of Materials Science, 29, p. 211, 1999

17. F. Bénédic, M. B. Assouar, F. Mohasseb, O. Elmazria, P. Alnot, A. Gicquel, "Surface Acoustic Wave Devices Based on Nanocrystalline Diamond and Aluminum Nitride," Diamond and Related Materials, 13, pp. 347-353, 2004

18. B. Bi, W. S. Huang, J. Asmussen, B. Golding, "Surface Acoustic Waves on Nanocrystalline Diamond," Diamond and Related Materials, 11, pp. 677-680, 2002

19. A. A. Oliner, G. W. Farnell, H. M. Gerard, E. A. Ash, A. J. Sloabodnik, Jr., H. I. Smith, Topics in Applied Physics: Acoustic Surface Waves, Vol. 24, Springer-Verlag, Berlin, Heidelberg, New York 1978

20. B. A. Auld, Acoustic Fields and Waves in Solids, Vol. 1, John Wiley & Sons, New York 1973

21. L. Solymar, D. Walsh, Lectures on the Electrical Properties of Materials, Oxford University Press, New York 1988

22. C. M. Flannery, M. D. Whitfield, R. B. Jackman, "Acoustic Wave Properties of CVD Diamond," Semiconductor Science and Technology, 18, pp. S86-S95, 2003

23. O. Elmazria, V. Mortet, M. El Hakiki, M. Nesladek, P. Alnot, "High Velocity SAW Using Aluminum Nitride Film on Unpolished Nucleation Side of Free-Standing CVD Diamond," IEEE Transactions on Ultrasonics, Ferroelectrics and Frequency Control, Vol. 50, No. 6, pp. 710-715, Jun. 2003

24. T. Lamara, M. Belmahi, O. Elmazria, L. Le Brizoual, J. Bougdira, M. Rémy, P. Alnot, "Freestanding CVD Diamond Elaborated By Pulsed-Microwave-Plasma for ZnO/Diamond SAW Devices," Diamond and Related Materials, 13, pp. 581-584, 2004

25. M. Ishihara, T. Nakamura, F. Kokai, Y. Koga, "Preparation of AlN and $LiNbO_3$ Thin films on Diamond Substrates By Sputtering Method," Diamond and Related Materials, 11, pp. 408-412, 2002

26. M. B. Assouar, O. Elmazria, L. Le Brizoual, P. Alnot, "Reactive DC Magnetron Sputtering of Aluminum Nitride Films for Surface Acoustic Wave Devices," Diamond and Related Materials, 11, pp. 413-417, 2002

27. T. Makkonen, V. P. Plessky, W. Steichen, W. Steichen, "Surface-Acoustic-Wave Devices for the 2.5-5 GHz Frequency Range Based on Longitudinal Leaky Waves," Applied Physics Letters, Vol. 82, No. 19, pp. 3351-3353, May 2003

28. G. G. Iriarte, G. Engelmark, I. V. Katardjiev, V. Plessky, V. Yantchev, "SAW COM-Parameter Extraction in AlN/Diamond Layered Structures," IEEE Transactions on Ultrasonics, Ferroelectrics and Frequency Control, Vol. 50, No. 11, pp. 1542-1547, Nov. 2003

29. A Frass, G. Lehmann, A. Lomonosov, P. Hess, "Linear and Nonlinear Elastic Surface Waves: From Seismic Waves to Material Science," Analytical Sciences, Vol. 17, pp S9-S12, Apr. 2001

30. M. Benetti, D. Cannatà, F. Di Pietrantonio, E. Verona, " Growth of AlN Piezoelectric Film on Diamond for High-Frequency Surface Acoustic Wave Devices," IEEE Transactions on Ultrasonics, Ferroelectrics and Frequency Control, Vol. 52, No. 10, pp. 1806-1811, Oct. 2005

31. B. Chapman, Glow Discharge Processes, John Wiley & Sons, New York 1980

32. D. Carter, H. Walde, G. McDonough, G. Roche, "Parameter Optimization in Pulsed DC Reactive Sputter Deposition of Aluminum Oxide," Society of Vacuum Coaters, pp. 570-577, 2002

33. A. Belkind, A. Freilich, J. Lopez, Z. Zhao, W. Zhu, K. Becker, "Characterization of Pulsed DC Magnetron Sputtering Plasmas," New Journal of Physics, Vol. 7, No. 90, pp. 2-15, Apr. 2005

34. Kurt J. Lesker Operation Manual PVD Series, Version

35. Advanced Energy User Manual MDX 1.5K Magnetron Drive, Apr. 1997

36. Advanced Energy User Manual Sparc-le V 100 kHz, Nov. 2002

37. Kurt J. Lesker M.A.P.S. Power Supply Installation and Operation Manual, Version 1.2

38. Watlow Series SD User's Manual PID Controller and PID Profiling Controller, Apr. 2004

39. Watlow Series SD User's Manual Limit Controller, Dec. 2002

40. Kurt J. Lesker TORUS Magnetron Sputtering Sources Installation and Operation Manual, Version 2.2

41. M. B. Assouar, O. Elmazria, M. Elhakiki, P. Alnot, "Study of Structural and Microstructural Properties of AlN Films Deposited On Silicon and Quartz Substrates For Surface Acoustic Wave Devices," Journal of Vacuum Science and Technology B, Vol. 22, No. 4, pp. 1717-1722, Jul./Aug. 2004

42. F. Engelmark, G. F. Iriarte, I. V. Katardjiev, M. Ottosson, P. Muralt, S. Berg, "Structural and Electroacoustic Studies of AlN Thin Films During Low Temperature Radio Frequency Sputter Deposition," Journal of Vacuum Science and Technology A, Vol. 19, No. 5, pp. 2664-2669, Sept./Oct. 2001

43. D. M. Pozar, Microwave Engineering, Addison-Wesley, Reading, MA, 1990, p. 221.

44. Hewlett Packard User's Manual HP 8753D Network Analyzer, Dec. 1997

45. Cascade Microtech Inc., 2430 NW 206th Avenue, Beaverton, Oregon 97006, USA

46. ECS Inc. International, ECS-D479.5B/D480A Series SAW Filter Data Sheet, 1105 S. Ridgeview, Olathe, KS 66062, USA